

# Direct generation of time-energy-entangled W triphotons in atomic vapor

Kangkang Li<sup>1</sup>, Jianming Wen<sup>2\*</sup>, Yin Cai<sup>1\*</sup>, Saeid Vashahri Ghamsari<sup>2</sup>, Changbiao Li<sup>1</sup>, Feng Li<sup>1</sup>, Zhaoyang Zhang<sup>1</sup>, Yanpeng Zhang<sup>1\*</sup>, and Min Xiao<sup>3,4</sup>

<sup>1</sup>Key Laboratory for Physical Electronics and Devices of the Ministry of Education & Shaanxi Key Lab of Information Photonic Technique, Xi'an Jiaotong University, Xi'an 710049, China

<sup>2</sup>Department of Physics, Kennesaw State University, Marietta, Georgia 30060, USA

<sup>3</sup>National Laboratory of Solid State Microstructures, College of Engineering and Applied Sciences and School of Physics, Nanjing University, Nanjing 210093, China

<sup>4</sup>Department of Physics, University of Arkansas, Fayetteville, Arkansas 72701, USA

\*emails: [jianming.wen@kennesaw.edu](mailto:jianming.wen@kennesaw.edu); [caiyin@xjtu.edu.cn](mailto:caiyin@xjtu.edu.cn); [ypzhang@mail.xjtu.edu.cn](mailto:ypzhang@mail.xjtu.edu.cn).

**Sources of entangled multiphotons are not only essential for fundamental tests of quantum foundations, but are also the cornerstone of a variety of optical quantum technologies today. Over past three decades, tremendous efforts have been devoted to creating multiphoton entanglement by multiplexing existing biphoton sources with linear optics and postselections. Different from all previous protocols, here we report, for the first time, the observation of continuous-mode time-energy-entangled W-class triphotons with an unprecedented generation rate directly through the process of spontaneous six-wave mixing (SSWM) in a four-level triple- $\Lambda$  atomic vapor cell. Facilitated by electromagnetically induced transparency and coherence control, our SSWM scheme enables versatile narrowband triphoton generation with many intriguing properties including long temporal coherence and controllable waveforms, ideal for implementing long-distance quantum communications, networking, and information processing by interfacing photons and atoms. Most importantly, our work paves a way for the development of a reliable and efficient genuine triphoton source, thus making the research on multiphoton entanglement within easy reach.**

Generating entangled multiphoton states<sup>1</sup> is pivotal to probe quantum foundations and advance technological innovations. Comprehensive studies have already shown that multiphoton entanglement<sup>1</sup> enables a plethora of classically impossible phenomena, most of them incomprehensible with any bipartite system. Unfortunately, we hitherto have at hand only biphoton sources based upon spontaneous parametric down-conversion (SPDC) or spontaneous four-wave mixing (SFWM). This has urged tremendous efforts on developing multiphoton sources<sup>1-3</sup> over past thirty years. Among them, the most popular means is to multiplex existing biphoton sources with linear optics and postselections. This brings us the well-known exemplar of polarization-entangled multiphotons<sup>4-8</sup> by constructing imperative interferometric setups. Although postselection might be acceptable in some protocols, it is generally deleterious for most applications since the action of observing photons alters and destroys the states. To avoid postselection, the second path considers cascaded SPDCs/SFWMs<sup>9-12</sup> or two SPDCs/SFWMs followed by one up-conversion<sup>13,14</sup>. In this way, polarization or time-energy entangled triphotons were reported by building sophisticated coincidence counting circuits. Despite no needs on interferometric settings, the attained states are intrinsically non-Gaussian due to unbalanced

photon numbers between the primary and secondary biphoton process, thereby making these sources very noisy and inefficient. Alternatively, the third technique<sup>15-17</sup> suggests to coherently mix paired photons with singles attenuated from a cw laser to trigger triphoton events. Akin to the first method, this solution depends on erasing the photon distinguishability by resorting to the Hong-Ou-Mandel interference effect<sup>18</sup>. Though polarization-entangled multiphotons of inequivalent classes were experimented with postselection, the low success rate and required interferometric stabilization make this proposal not so practical. As photons are always emitted in pairs in SPDC/SFWM, this attribute results in the fourth route<sup>19-21</sup> to make use of emission of multiple pairs by appropriately setting input pump powers. Though it seems easy to yield even-number states, yet, dominant biphotons from lower-order perturbation of the parametric process challenge detecting entangled multiphotons from higher-order perturbations. To have an acceptable fidelity, like the second way, a complicated detection system plus an interferometric setup is often inevitable in practice. What's more, this approach mainly allows to form polarization entanglement thus far. In spite of these impressive achievements, all foregoing mechanisms are difficult to offer a reliable and efficient triphoton source for research and applications. Additionally, so far there is no convincing realization of the entangled triphoton experiment in continuous modes. Driven by SPDC, one would expect that such photons could be naturally born from third-order SPDC<sup>22,23</sup> by converting one pump photon of higher energy into three daughter photons of low energy. The idea looks simple and straightforward, but experimentally inaccessible owing to the lack of such a nonlinear optical material. As a result, developing a reliable triphoton source is still in its infancy even up to today.

Coherent atomic media<sup>24</sup>, on the other hand, exhibit a wide range of peculiar properties including giant nonlinearities, prolonged atomic coherence, strong photon-atom interaction, and slow/fast light effects. Recently, these exotic properties have been skillfully employed to construct a novel narrowband biphoton source<sup>25-28</sup> basing on SFWM. Specifically, giant nonlinearities promise efficient parametric conversion, long atomic coherence leads to narrowband wavepackets, and sharp optical response becomes a formidable knob for shaping photon waveforms and temporal correlations. Unlike solid state sources, one unique feature pertinent to atomic ensembles arises from the dual role played by the third-order nonlinear susceptibility  $\chi^{(3)}$  in biphoton generation<sup>25,29-31</sup>. That is, in addition to governing nonlinear conversion strength, the double-resonance structure in  $\chi^{(3)}$  signifies the coexistence of two sets of SFWMs in light quanta radiation. Alternatively, entangled photons output from these two stochastic but coherent SFWM processes interfere and give rise to a nontrivial two-photon interference, namely, the damped Rabi oscillations. In general, their waveforms are entirely patterned by the convolution of a complex phase-mismatch function and  $\chi^{(3)}$ . Other than these attributes, the nonclassical correlations shared by paired photons can be additionally manipulated by exploiting various coherent control techniques including electromagnetically induced transparency<sup>24</sup> (EIT) to reshape optical responses. The interplay amongst diverse effects also enriches fundamental research and fosters technological innovations, inaccessible to other existing biphoton sources. Besides, flexible system layouts like backward detection geometry are more favorable to photon counting detection. Motivated by these

advantages, here we move one step forward and report the direct generation of continuous-mode triphotons entangled in time and energy from a hot atomic vapor cell. By utilizing the process of spontaneous six-wave mixing<sup>32,33</sup> (SSWM), we have not only observed the striking three-photon interference but also witnessed the residual two-photon correlation by tracing one photon out, an intrinsic virtue of the W class of tripartite entanglement<sup>34</sup>. By adjusting the system parameters, we have further achieved waveform-controllable triphoton generation. Together with an unprecedented production rate, our scheme has substantiated to be the first reliable platform that leverages multipartite entanglement research to an unparalleled level.

As schematic in Figs. 1A-C, we are interested in yielding narrowband W triphotons from a 7-cm long <sup>85</sup>Rb vapor cell with a four-level triple- $\Lambda$  atomic configuration at temperature 80°C (or 115°C). The detail of the experimental setup is provided in Methods. In the presence of three counter-propagating cw laser beams (one weak pump ( $E_1, \omega_1, \vec{k}_1$ ) and two strong couplings ( $E_2, \omega_2, \vec{k}_2$ ) and ( $E_3, \omega_3, \vec{k}_3$ )), backward photon triplets ( $E_{sj}, \omega_{sj}, \vec{k}_{sj}$  with  $j = 1, 2, 3$ ) are emitted via Doppler-broadened SSWM at an intersection angle of  $\theta \approx 4^\circ$  to the principle z-axis along the phase matching direction,  $\Delta \vec{k} = (\vec{k}_{s1} + \vec{k}_{s2} + \vec{k}_{s3}) - (\vec{k}_1 + \vec{k}_2 + \vec{k}_3) = 0$ . As depicted in Figs. 1B and C, the three coaxial input lasers were coupled into the center of the <sup>85</sup>Rb vapor cell with tunable frequency detunings  $\Delta_j$  and powers  $P_j$ ; while the generated photon triplets were accordingly detected by three single-photon counting modules (SPCM<sub>1</sub> – SPCM<sub>3</sub>) for coincidence counts after spatial and frequency filtering. Here, to avoid unwanted accidental trigger events induced by singles and dual biphotons, we placed single-band filters and narrowband etalon Fabry-Perot cavities in front of SPCM<sub>j</sub> before detection. We notice that in three-photon joint clicks, the major source of accidental coincidences stems from double pairs from two different SFWMs simultaneously present in the detection system (Supplementary Information (SI)). Since these dual pairs may have similar central frequencies and polarizations as genuine triphoton modes, they cannot be filtered away simply by polarizers and frequency filters. To exclude such double-pair false trigger events, in experiment we further introduced an additional SPCM<sub>d</sub> synchronized with SPCM<sub>3</sub> to serve as the diagnosis detector in conjunction with the rest two, SPCM<sub>1</sub> and SPCM<sub>2</sub>. To ensure the atomic population to be mainly distributed in the ground level  $|5S_{\frac{1}{2}}, F = 2\rangle$  throughout the measurement, an additional strong optical repumping beam ( $E_{op}$ ) was applied to the atomic transition  $|5S_{\frac{1}{2}}, F = 3\rangle \rightarrow |5P_{\frac{1}{2}}\rangle$  in alignment with  $E_2$  but without spatial overlap. With these preparations, we carefully adjust the system parameters, especially  $P_j$  and  $\Delta_j$  of each input field  $E_j$ , to promote the SSWM occurrence.

Physically, the SSWM process can be understood from the effective interaction Hamiltonian

$$H = \epsilon_0 \int_V d^3r \chi^{(5)} E_1 E_2 E_3 E_{S1}^{(-)} E_{S2}^{(-)} E_{S3}^{(-)} + H. c. \text{ (H. c., Hermitian conjugate),} \quad (1)$$

with three input (output) beams treated as classical (quantized) fields and  $V$  being the interaction volume. In Eq. (1),  $\chi^{(5)}$  denotes the fifth-order Doppler-broadened nonlinear susceptibility and governs the nonlinear conversion efficiency. In the Schrödinger picture, after some algebra, the triphoton state at the two cell surfaces can be derived from first-order perturbation theory by ignoring the vacuum contribution (SI), and takes the form of

$$|\Psi\rangle \propto \iiint d\omega_{S1} d\omega_{S2} d\omega_{S3} \chi^{(5)} \Phi\left(\frac{\Delta k L}{2}\right) \delta(\Delta\omega) |1_{\omega_{S1}}, 1_{\omega_{S2}}, 1_{\omega_{S3}}\rangle. \quad (2)$$

Here,  $\Delta\omega = \sum_{j=1}^3 (\omega_{Sj} - \omega_j)$ ,  $L$  is the interaction length,  $\Delta k = \Delta\vec{k} \cdot \hat{z}$  is the phase (or wavenumber) mismatch, the phase-mismatch longitudinal function  $\Phi(x) = \text{sinc}(x)e^{-ix}$  ascribes the three-photon natural spectral width arising from their different group velocities. Besides conditioning the triphoton output rate, the  $\chi^{(5)}$ -resonance profile also specifies the generation mechanism along with the photon intrinsic bandwidths. Overall, the state (2) outlines a few peculiar features yet to be experimentally verified: First, because of its non-factorization,  $|\Psi\rangle$  is entangled in frequency (or time), instead of polarization. Second, characterized by two independent variables,  $|\Psi\rangle$  conforms to the essential characteristics of the tripartite W class, that is, by tracing one photon away, partial entanglement still exists in the remaining bipartite subsystem. Third, since the triphoton waveform is defined by the convolution of  $\Phi$  and  $\chi^{(5)}$ , two distinct types of Glauber third-order (as well as conditional second-order) temporal correlations are expected to be manifested in threefold (and conditioned twofold) coincidence counting measurement. Consequently, two very differing scenarios are expected to be revealed in triphoton coincidence counting measurement. Last, but not the least, the triplet production rate is linear in the intensity of each input laser and can be dramatically enhanced by orders of magnitude by optimizing system parameters. It is worth pointing out that all these striking properties have been well affirmed in our series of experiments. Of importance, this is the first experimental proof of the time-energy-entangled triphoton W state discovered a decade ago<sup>34</sup> but never realized.

In experiment, we optimized the SSWM phase-matching condition via controlling the frequency detunings and incident angles of three driving fields so as to effectively collect emitted triphotons. Upon triggering SPCM<sub>j</sub>, the temporal correlation was concealed in photon counting histograms saved in a fast-time acquisition card with 0.0244-ns bin width, where, within in every time window of 195 ns, the detection of an  $E_{S1}$ -photon triggered the start of a coincidence event that ended with the detection of subsequent  $E_{S2}$ - and  $E_{S3}$ -photons. In most measurements, we collected the total trigger events over an hour and then analyzed the corresponding three-photon coincidences from the histogram in the parameter space  $(\tau_{21}, \tau_{31})$ , where  $\tau_{21} = \tau_2 - \tau_1$  and  $\tau_{31} = \tau_3 - \tau_1$  are respectively the relative time delays with  $\tau_j$  being the triggering time of the SPCM<sub>j</sub>.

As an exemplar of such, Fig. 2A displays one set of measured threefold coincidence counts from one recorded histogram after subtracting the accidental noise, giving rise to an intriguing three-dimensional temporal correlation with the 18.6- and 19.0-ns effective measurement time window

along the  $\tau_{21}$ - and  $\tau_{31}$ -axis because of the employed detectors. For the 0.25-ns time-bin width per detector, integrating all involved time bins yields the total of  $\sim 6 \times 10^3$  threefold trigger events, which result in a raw triphoton generation rate of  $102 \pm 9$  per minute without account of the coupling loss and detection efficiency. This rate is orders of magnitude higher than any previous one, and can be further improved by applying more efficient SPCMs as well as optimizing the fiber coupling efficiency. From the raw data, the background accidentals were estimated to be  $6 \pm 1$  per minute, mainly originating from the residual dual pairs as well as accidental coincidences of uncorrelated singles and dark counts of the SPCMs. This low background noise implies that the undesired third-order nonlinear processes were well filtered out in the experiment. On the other hand, the complicated pattern is a direct consequence of nontrivial W-triphoton interferences due to the occurrence of multiple coexisting SSWM processes in the regime of damped Rabi oscillations. As described previously, these processes arise from the multi-resonance structure of  $\chi^{(5)}$ . According to our dressed-state calculations (SI), there are four such coexisting channels, as schematic in Fig. 2B, coherently contributing to the observed quantum interference. To confirm that the emitted triphoton state belongs to the W class, we then used the acquired data to investigate the correlation properties of different bipartite subsystems. To do so, we integrated the coincidence counts by tracing away one photon from every triphoton event over that photon's arrival time. In this way, we acquired the conditional two-photon temporal waveforms with  $\tau_{21}$  or  $\tau_{31}$  as variables, and plotted them, respectively, in Figs. 2C and D. Interestingly, the conditioned  $\tau_3$ -waveform in Fig. 2D exhibits a damped periodic oscillation with a period of  $\sim 6.2$  ns (SI); while the  $\tau_{21}$ -waveform in Fig. 2C reveals two superimposed damped periodic oscillations with another 1.7-ns period in addition to the 6.2-ns one (SI), an interference effect unusual to any existing biphoton source. In contrast, the triphoton waveform has flexible temporal widths, for instance, 28 ns along the direction of  $\tau_{21} + \tau_{31} = 15$  ns (Fig. 2E). This contrasting phenomenon also supports our theoretical picture from alternative aspect, that the observed interference is caused by at least three sets of coherently coexisting SSWM processes. As demonstrated in SI, our qualitative analysis gives a good account of the experimental data.

Since the attributes of triphoton waveforms are dependent on the system parameters, this prompts us to manipulate and control their quantum correlations by means of tuning the input lasers as well as the atomic density or optical depth (OD). To this end, we carried out a series of experiments to tailor temporal correlation by shaping their waveforms by varying various parameters. Two sets of such representative experimental data are presented in Fig. 3. In comparison to Fig. 2A, Fig. 3A shows the steered waveform by reducing the power and frequency detuning of the input  $E_2$  laser. As one can see, the profile of the triphoton temporal correlation is dramatically changed in spite of the reduced generation rate  $77.4 \pm 7.8$  minute<sup>-1</sup>. Especially, the conditional two-photon coincidence counts manifest mono-periodic oscillations with the same period of 6.2 ns along both  $\tau_{21}$  and  $\tau_{31}$  directions, as illustrated in Figs. 3B and C. This is because, in this case, the Rabi frequency of  $E_2$  was tuned to be very close to that of  $E_3$ . As a consequence, half of the multiple resonances associated with the emission of  $E_{S2}$ -photons (Fig. 2B) become degenerate and share

the same spectrum. Likewise, the triphoton temporal coherence length along the  $\tau_{21} + \tau_{31} = 29$  ns direction is enlarged to 40 ns. On the other hand, triphoton interference can be also modulated by altering the phase-mismatch longitudinal function  $\Phi$  in Eq. (2). Akin to the biphoton generation, the phase mismatch  $\Delta k$  in  $\Phi$  is determined by the linear susceptibility of each mode in SSWM via the EIT slow-light effect. As showcased in Fig. 3D, by augmenting the OD from 4.6 to 45.7, the triphoton temporal correlation is considerably modified by the dispersion relation of the atomic vapor and falls into the group-delay regime. In addition to raising the production rate to  $125 \pm 11$  per minute, the oscillatory curvature is markedly suppressed and replaced by the overall decay envelopes. This transformation becomes more evident when examining the conditioned two-photon coincidence counts. By comparing Fig. 3F with Figs. 3B, C and E, one can see that the enhanced dispersion apparently smears the damped Rabi oscillations along the  $\tau_{21}$ -direction, implying that the narrower bandwidths defined by  $\Phi\left(\frac{\Delta k L}{2}\right)$  regulate the bandwidths dictated by  $\chi^{(5)}$  to obscure the interference amongst four sets of coexisting SSWM channels. Besides, the triphoton temporal coherence length along the direction of  $\tau_{21} + \tau_{31} = 50$  ns is also significantly prolonged up to 70 ns.

To reveal the nonclassicality of the W triphoton state, we continued to examine the violation of the Cauchy-Schwarz inequality<sup>35,36</sup> as well as the fringe visibilities of the observed Rabi oscillations. By normalizing the threefold coincidence events to the flat background counts along with the additional auto-correlation measurement of the collected  $E_{S1}$ ,  $E_{S2}$  and  $E_{S3}$  photons, we found that the Cauchy-Schwarz inequality is violated by a factor of  $250 \pm 55$  in Fig. 2A,  $154 \pm 43$  in Fig. 3A, and  $79 \pm 21$  in Fig. 3D. Note that here these values were optimized by filtering possible biphoton processes in measurement. Additionally, we observed that the fringe visibility of Fig. 2A can be as high as  $90 \pm 5\%$ .

In addition to the above experiments, it is also instructive to explore the triphoton production rate and temporal correlation width as a function of the input pump power for further understanding the proposed generation mechanism. This has motivated us to implement additional measurements and the experimental data is presented in Fig. 4. As one can see, indeed, the triphoton generation rate follows a linear growth in the input power  $P_2$  of the  $E_2$  field. For the temporal coherence length, we concentrated on the two-photon conditional coincidence counting along the  $\tau_{21}$  and  $\tau_{31}$  directions. From Fig. 4, it is not difficult to find that increasing  $P_2$  results in the reduction of the correlation time. This stems from the reduced slow-light effect when augmenting  $P_2$ . Note that Figs. 2A, 3A and 3D simply become one individual point in Fig. 4. Overall, our approach enables all-optical coherent manipulation to create the genuine triphotons with controllable waveforms.

In conclusion, we have for the first time observed the efficient W-triphoton emission directly through SSWM in a warm atomic vapor with a generation rate of about  $125 \pm 11 \text{ min}^{-1}$ . Moreover, due to the coexistence of multi-SSWMs, these time-energy-entangled W triphotons have resulted in various nontrivial three-photon temporal interferences. Furthermore, by manipulating the

system parameters, the triphoton temporal correlations can be flexibly engineered and tailored and demonstrate many peculiar characteristics inaccessible to all previous mechanisms. As a reliable source, it is expected to play a vital role in probing foundations of quantum theory and advancing various quantum-based technologies in information processing, communications, imaging, metrology, etc.

## References

1. Pan, J.-W., Chen, Z.-B., Lu, C.-Y., Weinfurter, H., Zeilinger, A. & Zukowski, M. Multiphoton entanglement and interferometry. *Rev. Mod. Phys.* **84**, 777-838 (2012).
2. Friis, N., Vitagliano, G., Malik, M. & Huber, M. Entanglement certification from theory to experiment. *Nat. Rev. Phys.* **1**, 72-87 (2019).
3. Erhard, M., Krenn, M. & Zeilinger, A. Advances in high-dimensional quantum entanglement. *Nat. Rev. Phys.* **2**, 365-381 (2020).
4. Bouwmeester, D., Pan, J.-W., Daniell, M., Weinfurter, H. & Zeilinger, A. Observation of three-photon Greenberger-Horne-Zeilinger entanglement. *Phys. Rev. Lett.* **82**, 1345-1349 (1999).
5. Pan, J.-W., Bouwmeester, D., Gasparoni, S., Weihs, G. & Zeilinger, A. Experimental demonstration of four-photon entanglement and high-fidelity teleportation. *Phys. Rev. Lett.* **86**, 4435-4439 (2001).
6. Eibl, M., Kiesel, N., Bourennane, M., Kurtsiefer, C. & Weinfurter, H. Experimental realization of a three-qubit entangled W state. *Phys. Rev. Lett.* **92**, 077901 (2004).
7. Kiesel, N., Schmid, C., Toth, G., Solano, E. & Weinfurter, H. Experimental observation of four-photon entangled Dicke state with high fidelity. *Phys. Rev. Lett.* **98**, 063604 (2007).
8. Reimer, C., Kues, M., Roztock, P., Wetz, B., Grazioso, F., Little, B. E., Chu, S. T., Johnson, T., Bromberg, Y., Caspani, L., Moss, D. J. & Morandotti, R. Generation of multiphoton entangled quantum states by means of integrated frequency combs. *Science* **351**, 1176-1180 (2016).
9. Wen, J., Oh, E. & Du, S. Tripartite entanglement generation via four-wave mixings: narrowband triphoton W state. *J. Opt. Soc. Am. B* **27**, A11-A20 (2010).
10. Hubel, H., Hamel, D. R., Fedrizzi, A., Ramelow, S., Resch, K. J. & Jennewein, T. Direct generation of photon triplets using cascaded photon-pair sources. *Nature* **466**, 601-603 (2010).
11. Shalm, L. K., Hamel, D. R., Yan, Z., Simon, C., Resch, K. J. & Jennewein, T. Three-photon energy-time entanglement. *Nat. Phys.* **9**, 19-22 (2013).
12. Hamel, D. R., Shalm, L. K., Hubel, H., Miller, A. J., Marsili, F., Verma, V. B., Mirin, R. P., Nam, S. W., Resch, K. J. & Jennewein, T. Direction generation of three-photon polarization entanglement. *Nat. Photon.* **8**, 801-807 (2014).
13. Keller, T. E., Rubin, M. H., Shih, Y. & Wu, L.-A. Theory of the three-photon entangled state. *Phys. Rev. A* **57**, 2076-2079 (1998).
14. Wen, J., Xu, P., Rubin, M. H. & Shih, Y. Transverse correlations in triphoton entanglement: Geometrical and physical optics. *Phys. Rev. A* **76**, 023828 (2007).

15. Rarity, J. & Tapster, P. Three-particle entanglement from entangled photon pairs and a weak coherent state. *Phys. Rev. A* **59**, R35-R38 (1999).
16. Zhao, Z., Chen, Y.-A., Zhang, A.-N., Yang, T., Briegel, H. J. & Pan, J.-W. Experimental demonstration of five-photon entanglement and open destination teleportation. *Nature* **430**, 54-58 (2004).
17. Mikami, H., Li, Y., Fukuoka, K. & Kobayashi, T. New high-efficiency source of a three-photon W state and its full characterization using quantum state tomography. *Phys. Rev. Lett.* **95**, 150404 (2005).
18. Hong, C. K., Ou, Z. Y. & Mandel, L. Measurement of subpicosecond time intervals between two photons by interference. *Phys. Rev. Lett.* **59**, 2044-2046 (1987).
19. Eibl, M., Gaertner, S., Bourennane, M., Kurtsiefer, C., Zukowski, M. & Weinfurter, H. Experimental observation of four-photon entanglement from parametric down-conversion. *Phys. Rev. Lett.* **90**, 200403 (2003).
20. de Riedmatten, H., Scarani, V., Marcikic, I., Acin, A., Tittel, W., Zbinden, H. & Gisin, N. Two independent photon pairs versus four-photon entangled states in parametric down conversion. *J. Mod. Opt.* **51**, 1637-1649 (2003).
21. Bourennane, M., Eibl, M., Gaertner, S., Kurtsiefer, C., Cabello, A. & Weinfurter, H. Decoherence-free quantum information processing with four-photon entangled states. *Phys. Rev. Lett.* **92**, 107901 (2004).
22. Corna, M., Garay-Palmett, K. & U'Ren, A. B. Experimental proposal for the generation of entangled photon triplets by third-order spontaneous parametric downconversion. *Opt. Lett.* **36**, 190-192 (2011).
23. Borshchevskaya, N. A., Katamadze, K. G., Kulik, S. P. & Fedorov, M. V. Three-photon generation by means of third-order spontaneous parametric down-conversion in bulk crystals. *Laser Phys. Lett.* **12**, 115404 (2015).
24. Fleischhauer, M., Imamoglu, A. & Marangos, J. P. Electromagnetically induced transparency: Optics in coherent media. *Rev. Mod. Phys.* **77**, 733-673 (2005).
25. Du, S., Wen, J. & Rubin, M. H. Narrowband biphoton generation near atomic resonance. *J. Opt. Soc. Am. B* **25**, C98-C108 (2008).
26. Balic, V., Braje, D. A., Kolchin, P., Yin, G. Y. & Harris, S. E. Generation of pairs photons with controllable waveforms. *Phys. Rev. Lett.* **94**, 183601 (2005).
27. Du, S., Kolchin, P., Belthangady, C., Yin, G. Y. & Harris, S. E. Subnatural linewidth biphotons with controllable temporal length. *Phys. Rev. Lett.* **100**, 183603 (2008).
28. Shu, C., Chen, P., Chow, T. K. A., Zhu, L., Xiao, Y., Loy, M. M. T. & Du, S. Subnatural-linewidth biphotons from a Doppler-broadened hot atomic vapor cell. *Nat. Commun.* **7**, 12783 (2016).
29. Wen, J., Du, S. & Rubin, M. H. Biphoton generation in a two-level atomic ensemble. *Phys. Rev. A* **75**, 033809 (2007).
30. Wen, J., Du, S. & Rubin, M. H. Spontaneous parametric down-conversion in a three-level system. *Phys. Rev. A* **76**, 013825 (2007).



31. Wen, J., Du, S., Zhang, Y., Xiao, M. & Rubin, M. H. Nonclassical light generation via a four-level inverted-Y system. *Phys. Rev. A* **77**, 033816 (2008).
32. Kang, H., Hernandez, G. & Zhu, Y. Slow-light six-wave mixing at low light intensities. *Phys. Rev. Lett.* **93**, 073601 (2004).
33. Zhang, Y., Brown, A. W. & Xiao, M. Opening four-wave mixing and six-wave mixing channels via dual electromagnetically induced transparency windows. *Phys. Rev. Lett.* **99**, 123603 (2007).
34. Wen, J. & Rubin, M. H. Distinction of tripartite Greenberger-Horne-Zeilinger and W states entangled in time (or energy) and space. *Phys. Rev. A* **79**, 025802 (2009).
35. Reid, M. D. & Walls, D. F. Violations of classical inequalities in quantum optics. *Phys. Rev. A* **34**, 1260-1276 (1986).
36. Belinskii, A. V. & Klyshko, D. N. Interference of light and Bell's theorem. *Phys.-Usp.* **36**, 653-693 (1993).

## Acknowledgements

We are grateful to Xinghua Li, Dan Zhang, and Da Zhang for their contributions at the early stage of the project and to Yanhua Zhai for helpful discussions on the detection system. This research was supported by the National Key Research and Development Program of China (2017YFA0303700, 2018YFA0307500), Key Scientific and Technological Innovation Team of Shaanxi Province (2021TD-56), National Natural Science Foundation of China (61975159, 12174302, 62022066, 12074306, 12074303).

## Author Contributions

Y.Z. and J.W. conceived the idea and supervised the project with the help from Y.C. K.L., supervised by J.W. and Y.Z., performed the experiment, theoretical derivations, and numerical calculations with the help from S.V.G. J.W., K.L. and Y.Z. wrote the manuscript with contributions from all other authors. All contributed to the discussion of the project and analysis of experimental data.

## List of Figures

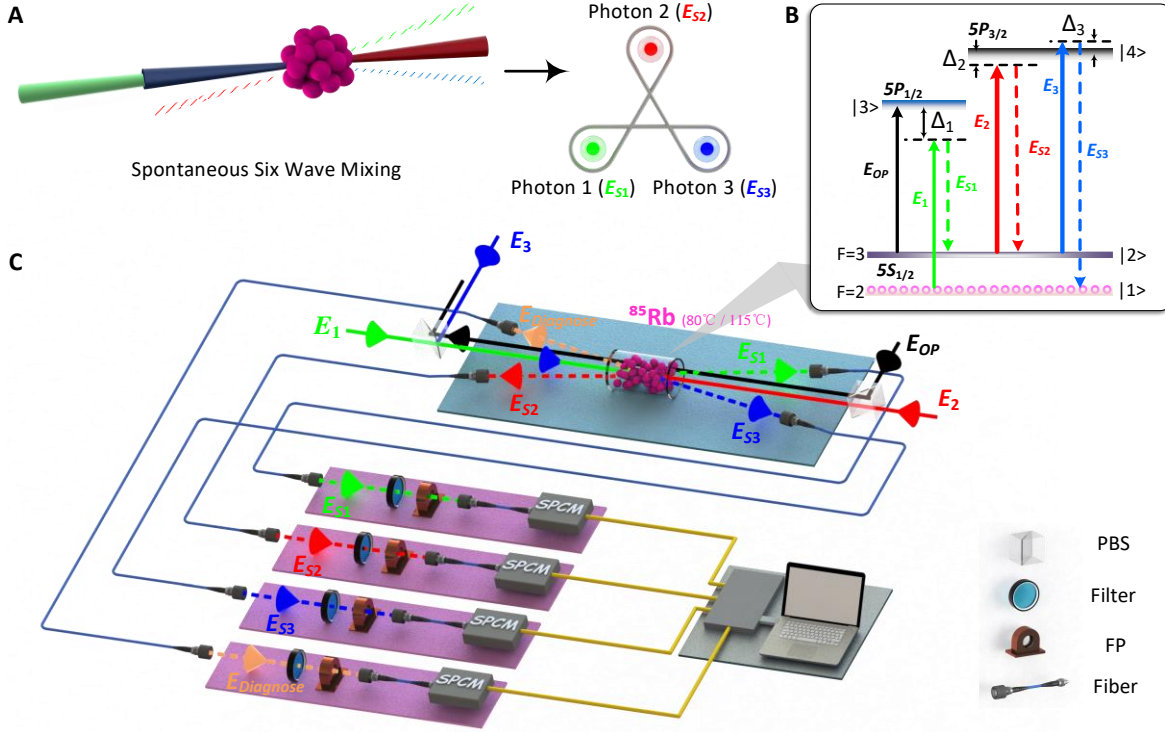


**Fig. 1. Generation of genuine W-triphotons entangled in time-energy directly via SSWM in a hot atomic vapor.** (A) Conceptual schematic of creating a W-triphoton state via the fifth-order parametric nonlinear process. (B) The  $^{85}\text{Rb}$  energy-level diagram of the SSWM process. (C) The experimental setup. Three coaxial input driving fields  $E_1$  (795 nm),  $E_2$  (780 nm) and  $E_3$  (780 nm) are coupled into the center of an  $^{85}\text{Rb}$  vapor cell heated at 80°C (or 115°C) to initiate the simultaneous generation of W-triphotons in  $E_{S1}$ ,  $E_{S2}$  and  $E_{S3}$ . An additional optical-pumping beam  $E_{OP}$  is added to clean up the residual atomic population in the level  $|2\rangle$  for preventing the noise from the Raman scattering. The generated photons are coupled into a data acquisition system by single-mode fibers and jointly detected by three synchronized single-photon counting modules (SPCM) with filters (F) and Fabry-Perot cavities (FP) placed in front. To eliminate accidental coincidences caused by dual biphotons and quadruphotons, an extra detection of the diagnosis photons  $E_{\text{Diagnose}}$  is applied to ensure the natural triphoton collection. All trigger events are then interrogated by a fast-time acquisition card with a computer.

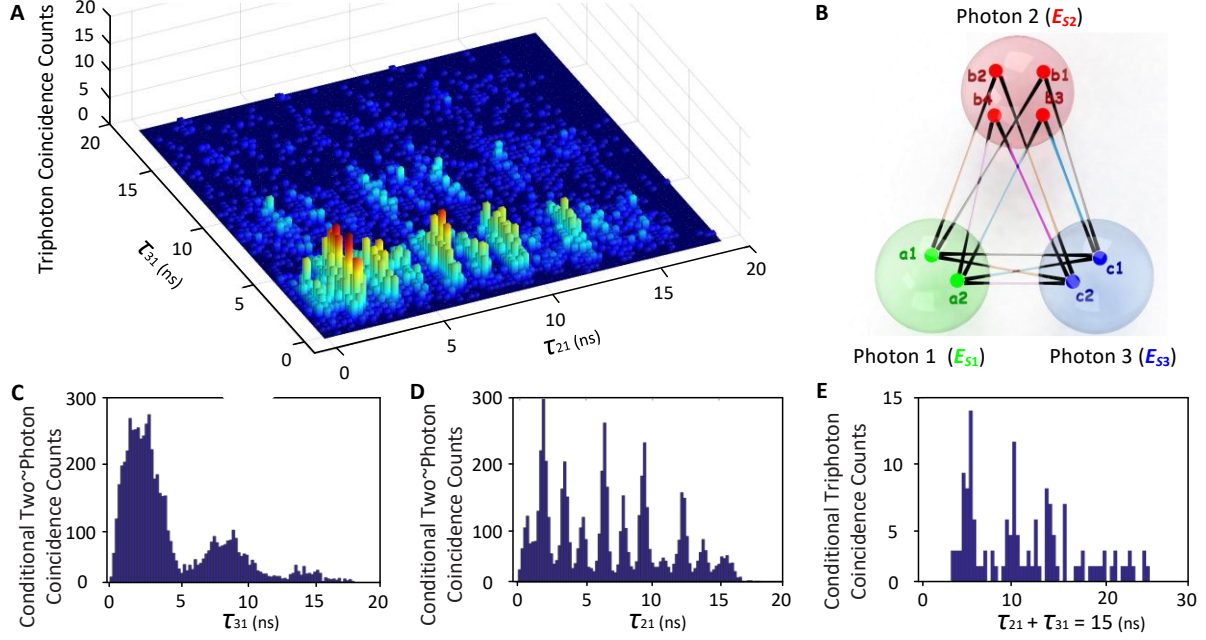


**Fig. 2. Triphoton coincidence counting measurements.** (A) Three-dimensional (3D) quantum interference formed by three-photon coincidence counts collected in 1 h with the time-bin width of 0.25 ns for OD = 4.6. The generation rate and accidentals are respectively  $102 \pm 9$  and  $6 \pm 1$  per minute. The powers of the input  $E_1$ ,  $E_2$  and  $E_3$  beams are  $P_1 = 4$  mW,  $P_2 = 40$  mW, and  $P_3 = 15$  mW, respectively, and the corresponding frequency detunings are  $\Delta_1 = -2$  GHz,  $\Delta_2 = -150$  MHz, and  $\Delta_3 = 50$  MHz. (B) Schematic illustration of triphoton interference originating from the coexistence of multi-SSWMs. (C) & (D) Conditional two~photon coincidence counts as the function of  $\tau_{21}$  and  $\tau_{31}$  in (A) by tracing the third photon  $E_{S3}$  and  $E_{S2}$ , respectively. (E) Conditional three-photon coincidence counts along the trajectory of  $\tau_{21} + \tau_{31} = 15$  ns in (A).

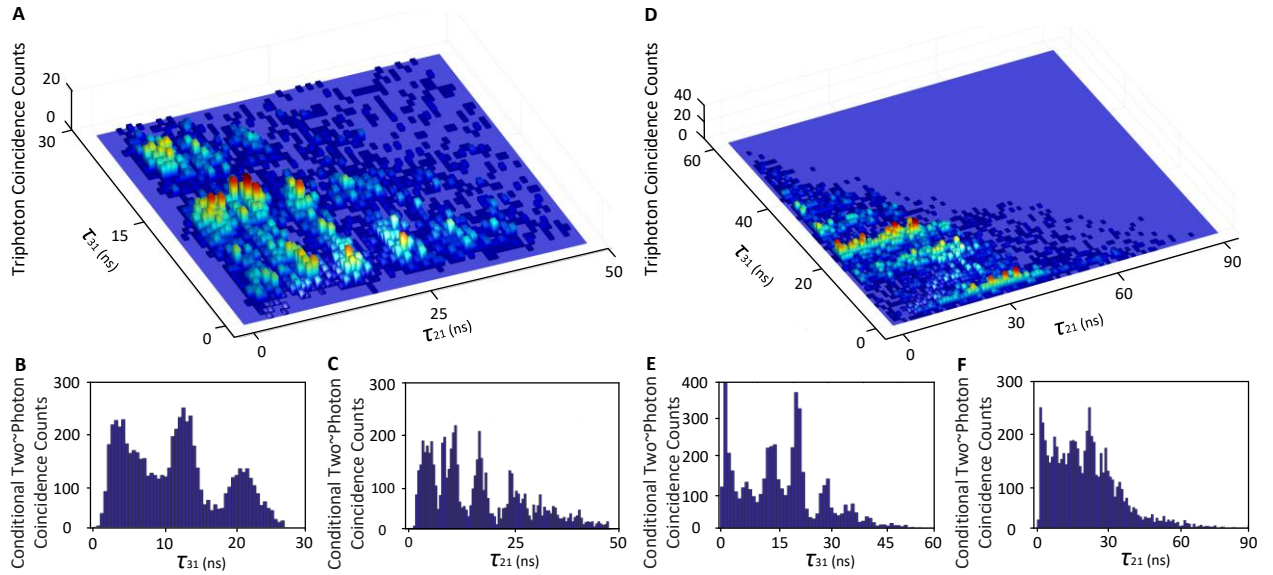


**Fig. 3. Triphoton coincidence counting measurements by tuning the coupling strength and OD.** (A) 3D quantum interference formed by three-photon coincidence counts collected in 1h with the 0.7-ns time-bin width by changing  $P_2$  to 15 mW and  $\Delta_2$  to  $-50$  MHz. Other parameters are same as Fig. 2. The generation rate and accidentals rate are  $77.4 \pm 7.8$  and  $11 \pm 2.1$  per minute, respectively. (B) & (C) Conditional two~photon coincidence counts as the function of  $\tau_{21}$  and  $\tau_{31}$  in (A) by tracing the third photon  $E_{S3}$  and  $E_{S2}$ , respectively. (D) Collected over 40 min with 1-ns time-bin width by changing OD to 45.7. Other parameters are same as Fig. 2. The generation and accidentals rates are  $125 \pm 11$  and  $28 \pm 6.4$  per minute, respectively. (E) & (F) Conditional two~photon coincidence counts as the function of  $\tau_{21}$  and  $\tau_{31}$  in (D).

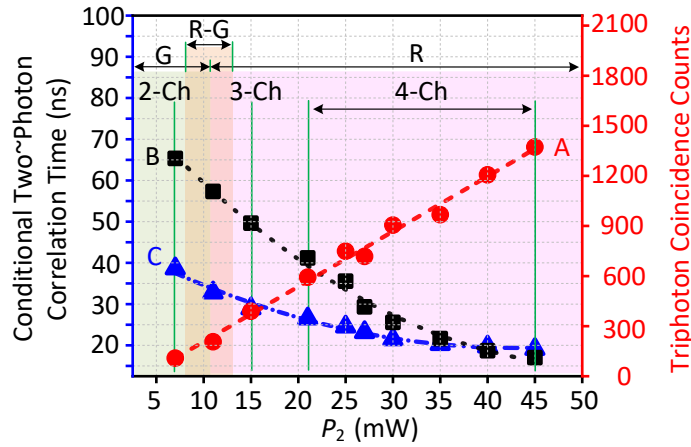


**Fig. 4. Controllable waveform generation.** The triphoton generation rate (red dots) in 15 minutes versus the input power  $P_2$  of the driving field  $E_2$ . The correlation times of conditional two~photon coincidences along the  $\tau_{21}$  (black squares) and  $\tau_{31}$  (blue triangles) directions by changing  $P_2$ . By increasing  $P_2$ , the triphoton temporal correlation is shifted from the group-delay (G) regime to the Rabi-oscillation (R) region.  $j$ -Ch ( $j = 2,3,4$ ) means the coherent coexistence of  $j$  types of indistinguishable SSWMs. The experimental condition is same as that in Fig 2.

## Methods

**Experimental implementation.** Experimentally, three coaxial driving beams  $E_1$ ,  $E_2$  and  $E_3$  are coupled to the center of the  $^{85}\text{Rb}$  vapor cell to initiate the SSWM process, as shown in Fig. 2. The relevant energy-level diagram is shown in Fig. 1B, where the atoms are prepared at the ground level  $|1\rangle$  ( $5S_{1/2}, F = 2$ ). The other involved energy levels are  $|2\rangle$  ( $5S_{1/2}, F = 3$ ),  $|3\rangle$  ( $5P_{1/2}$ ), and  $|4\rangle$  ( $5P_{3/2}$ ). The horizontally polarized weak probe  $E_1$  beam at the 795-nm wavelength is applied the atomic transition  $|1\rangle \rightarrow |3\rangle$  with a large red frequency detuning  $\Delta_1$  (2 GHz) so that the atomic population resides primarily at  $|1\rangle$ . The other two strong coupling beams  $E_2$  (780 nm, horizontal polarization) and  $E_3$  (780 nm, vertical polarization) are near resonantly coupled to the same atomic

transition  $|2\rangle \rightarrow |4\rangle$  but with changeable detunings  $\Delta_2$  and  $\Delta_3$ . By carefully adjusting the phase matching conditions, the spatially separated triphotons  $E_{S1}$ ,  $E_{S2}$  and  $E_{S3}$  with wave vectors  $\vec{k}_{S1}$ ,  $\vec{k}_{S2}$  and  $\vec{k}_{S3}$  are spontaneously emitted along the phase-matching directions with a small forward angle about  $4^\circ$  away from the three driving fields. Besides, we have added an additional optical-pumping beam  $E_{OP}$  to clean up the residue atomic population in  $|2\rangle$  so that the Raman scattering can be suppressed from the transition  $|2\rangle \rightarrow |3\rangle$ . To increase the fifth-order nonlinearity, the  $^{85}\text{Rb}$  vapor cell with a length of  $L = 7$  cm is heated to  $80^\circ\text{C}$  (or  $115^\circ\text{C}$ ). In this regard, the reported data in Figs. 2 and 3A-C were collected at the temperature of  $80^\circ\text{C}$ ; while the data presented in Figs. 3D-F were obtained at  $115^\circ\text{C}$ . Also, the narrowband filters and customized interference etalon Fabry-Perot (FP) cavities are placed in front of each SPCM to filter the scattered driving lasers from the collected triphoton trigger events. After detected by SPCMs, the trigger events are recorded by a time-to-digit converter, where the maximum resolution time of our recording card is 813 fs. In our experiment, the fiber-fiber coupling efficiency and the SPCM detection efficiency are 70% and 40%, respectively.

**Filtering possible biphoton processes from triphoton coincidence counts.** Although the triphoton generation by SSWM is the focus of the measurement, due to the larger magnitude of the third-order nonlinearity, it is necessary to consider the possible false counts from the biphoton processes. Based on the atomic level structure and the adopted field coupling geometry, there are seven crucial SFWMs (Fig. S6 in SI) that may result in accidental coincidences: (1) SFWM1 initiated by  $E_1$  and  $E_2$ , (2) SFWM2 by  $E_1$  and  $E_3$ , (3) SFWM3 by  $E_2$  and  $E_3$ , (4) SFWM4 by  $E_3$  and  $E_2$ , (5) SFWM5 by  $2E_1$ , (6) SFWM6 by  $2E_2$ , and (7) SFWM7 by  $2E_3$ . Specifically, the biphotons produced from the following SFWMs may contribute to the accidental joint-detection probability: (1) SFWM1 + SFWM2, (2) SFWM1 + SFWM3, (3) SFWM1 + SFWM4, (4) SFWM1 + SFWM5, (5) SFWM1 + SFWM7, (6) SFWM2 + SFWM3, (7) SFWM2 + SFWM4, (8) SFWM2 + SFWM6, (9) SFWM3 + SFWM4, (10), SFWM3 + SFWM5, (11) SFWM3 + SFWM7, (12) SFWM4 + SFWM5, (13) SFWM4 + SFWM7, (14) SFWM5 + SFWM6, and (15) SFWM6 + SFWM7. Fortunately, the central frequency difference of the similar photons from SSWM and SFWMs are more than 3 GHz. Therefore, before being detected by SPCMs, the collected photons need to pass through the high-quality single-frequency band filters and the customized narrowband etalon Fabry-Perot cavity (with a bandwidth  $\sim 600$  MHz). The bandwidth, transmission efficiency, and extinction ratio of the employed filters are 650 MHz, 80%, and 60 dB, respectively. After these measures, most of the biphoton noise can be filtered from the detection. In addition, the phase-matching condition for the SSWM process is much different from those for the possible SFWM processes. For instance, the photons from SFWM2 have distinctive emission angles from those from SSWM. As a result, the three-photon coincidence counts in actual measurements are mainly determined by true triphotons, uncorrelated singles, and dark counts. In practice, the biphotons and uncorrelated singles can be well filtered in the three-photon coincidence counting measurement by carefully adjusting the phase-matching conditions.

**Additional detection of diagnose photons  $E_{\text{Diagnose}}$ .** To further guarantee the detected photons that are really from SSWM, we have performed one additional detection of the two-photon coincidences  $E_{S3}$  and  $E_{\text{Diagnose}}$  simultaneously in conjunction with the coincidences between  $E_{S1}$  and  $E_{S2}$  by artificially introducing the diagnose photons  $E_{\text{Diagnose}}$ . This arrangement allows us to greatly reduce the false three-photon trigger events from dual biphotons particularly. The experimental results of  $E_{S3}$  and  $E_{\text{Diagnose}}$  are given in the SI. By the same reconstruction method, we notice that the trigger events from two pairs of biphotons can be safely removed from the data recording.

**The Cauchy-Schwarz inequality.** The nonclassicality of triphoton correlation can be verified by observing the violation of the well-known Cauchy-Schwarz inequality, which is defined by

$$\frac{[g^{(3)}(\tau_{21}, \tau_{31})]^2}{[g_{S1}^{(1)}]^2 [g_{S2}^{(1)}]^2 [g_{S3}^{(1)}]^2} \leq 1.$$

Here,  $g^{(3)}(\tau_2, \tau_3)$  is the normalized third-order correlation function with respect to the accidental background.  $g_{S1}^{(1)}$ ,  $g_{S2}^{(1)}$  and  $g_{S3}^{(1)}$  are the normalized autocorrelations of the emitted photons  $E_{S1}$ ,  $E_{S2}$  and  $E_{S3}$  measured by a fiber beam splitter. In our experiment, the nonzero background floor in such as Figs. 2 and 3 is a result of the accidental coincidences between uncorrelated single photons. According to the measured data, we estimate that the maximum values of  $g_{S1}^{(1)}$ ,  $g_{S2}^{(1)}$  and  $g_{S3}^{(1)}$  are respectively to be  $1.6 \pm 0.2$ , 2 and 2.

# Supplementary Information for “Direct generation of time-energy-entangled W triphotons in atomic vapor”

Kangkang Li<sup>1,5</sup>, Jianming Wen<sup>2\*</sup>, Yin Cai<sup>1\*</sup>, Saeid Vashahri Ghamsari<sup>2</sup>, Changbiao Li<sup>1</sup>, Feng Li<sup>1</sup>, Zhaoyang Zhang<sup>1</sup>, Yanpeng Zhang<sup>1\*</sup>, and Min Xiao<sup>3,4</sup>

<sup>1</sup>Key Laboratory for Physical Electronics and Devices of the Ministry of Education & Shaanxi Key Lab of Information Photonic Technique, Xi'an Jiaotong University, Xi'an 710049, China

<sup>2</sup>Department of Physics, Kennesaw State University, Marietta, Georgia 30060, USA

<sup>3</sup>National Laboratory of Solid State Microstructures, College of Engineering and Applied Sciences and School of Physics, Nanjing University, Nanjing 210093, China

<sup>4</sup>Department of Physics, University of Arkansas, Fayetteville, Arkansas 72701, USA

\*emails: [jianming.wen@kennesaw.edu](mailto:jianming.wen@kennesaw.edu); [caiying@xjtu.edu.cn](mailto:caiying@xjtu.edu.cn); [ypzhang@mail.xjtu.edu.cn](mailto:ypzhang@mail.xjtu.edu.cn).

- I. Theory of Time-Energy-Entangled W Triphoton Generation in an Atomic Vapor
    - Qualitative Derivation of Fifth-Order Nonlinear Susceptibility  $\chi^{(5)}$
    - Qualitative Derivations of Linear Susceptibilities  $\chi$
    - Derivation of the Triphoton W State  $|\Psi\rangle$
    - Derivations of Temporal Correlations of W Triphotons
    - Triphoton W State Entangled in Other Degrees of Freedom
  - II. Further Information on Experimental Measurements and Data Processing
    - Possible Biphoton Processes
    - Measured Coincidence Counts by Subtracting Background Accidentals
    - Reconstruction Procedure for Triphoton Coincidence Counts
    - Additional Experimental Data
  - III. Comparison of Various Mechanisms on Multiphoton Generation
  - IV. Further Discussion on the Reported Triphoton Source
- References

## I. Theory of Time-Energy-Entangled W Triphoton Generation in an Atomic Vapor

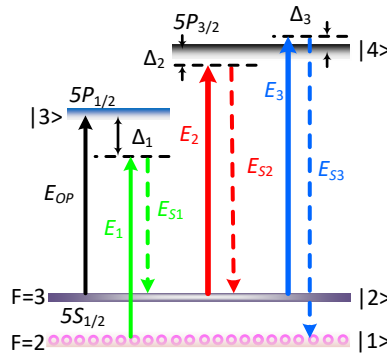


**Figure S1 | Energy-level diagram of hot <sup>85</sup>Rb atoms for direct generation of time-energy-entangled W-class triphotons.** The light-atom interaction in a four-level triple-Λ-type atomic configuration where the two ground states are denoted by |1> and |2>, and the two excited states by |3> and |4>. Initially, all

atomic population is prepared at  $|1\rangle$ . To ensure no residual atomic population to be distributed in  $|2\rangle$ , an additional optical pumping beam  $E_{OP}$  is applied resonantly with the atomic transition  $|2\rangle \leftrightarrow |3\rangle$ . A weak pump laser  $E_1$  is applied to  $|1\rangle \rightarrow |3\rangle$  with a large, fixed red frequency detuning  $\Delta_1$ , along with the simultaneous presence of another two strong control fields  $E_2$  and  $E_3$  applied to the same atomic transition  $|2\rangle \rightarrow |4\rangle$  but with different frequency detunings  $\Delta_2$  and  $\Delta_3$ . Under the demanded phase-matching conditions, the occurrence of the spontaneous six-wave mixing (SSWM) process will then enable the direct, efficient emission of continuous-mode time-energy-entangled W-type triphotons  $E_{S1}$ ,  $E_{S2}$  and  $E_{S3}$  from their respective atomic transitions as schematically sketched in the diagram.

### **Qualitative Derivation of Fifth-Order Nonlinear Susceptibility $\chi^{(5)}$**

Nonlinear optics is a cornerstone for generating, manipulating, and converting quantum light. When an atomic ensemble is utilized to generate nonclassical light, its optical response including both linear and nonlinear susceptibilities can play a decisive role in determining the properties of the produced quantum state and waveform. This is especially true when the light-atom interaction takes place near atomic resonance and the generated nonclassical light is much weaker than the input driving fields. As such, the primary task of this type of problems is to derive the linear and nonlinear susceptibilities for the participating electromagnetic (EM) fields. We notice that when only one EM field is involved per atomic transition, there are several ways such as density-matrix formalism and master equations to compute these susceptibilities. However, the situation becomes exceedingly complicated when more than one optical field acts onto the same atomic transition. For such a case, Wen and his coworkers have developed a useful methodology [1-3] which enables precise calculations on these susceptibilities. While this approach [1-3] in principle allows accurate calculations on optical responses, especially for the production of entangled paired photons, it becomes computationally cumbersome when applied to the triphoton generation considered in this work. We are currently working on the exact derivations using this method. But here we would like to use a qualitative means to study the triphoton emission as well as the associated optical properties. This qualitative method has previously been applied to some atomic systems with similar energy-level structures and coupling interactions [4-8] to ascribe six-wave mixing (SWM). As shall be shown below, despite the derived qualitative results cannot perfectly match the experimental data, they do provide a somewhat plausible explanation for the triphoton formation.

The underlying physics behind this qualitative method is rooted in the perturbation theory, which largely takes into account the dressing steady states but ignores the transient propagation effect. The first step is to perturbatively analyze the SWM process under the weak-field approximation. Then, the dressing perturbation is adopted to set up a set of the strong-field coupled equations to obtain the density-matrix elements through the perturbation chain rule. By following the similar calculations presented in Refs. [4-8], we found that the fifth-order nonlinear susceptibility  $\chi^{(5)}$  can be approximately attained from the following perturbation chain,

$$\rho_{11}^{(0)} \xrightarrow{\omega_1} \rho_{31}^{(1)} \xrightarrow{\omega_{S1}} \rho_{21}^{(2)} \xrightarrow{\omega_2} \rho_{41}^{(3)} \xrightarrow{\omega_{S2}} \rho_{11}^{(4)} \xrightarrow{\omega_3} \rho_{41}^{(5)}, \quad (S1)$$



where  $\omega_1, \omega_2$  and  $\omega_3$  are the three input laser frequencies, and  $\omega_{S1}, \omega_{S2}$  and  $\omega_{S3}$  are generated triphoton frequencies, respectively. By solving the series of density-matrix equations, one can find the density-matrix elements  $\rho_{11}^{(0)}, \rho_{31}^{(1)}, \dots, \rho_{41}^{(5)}$  in Eq. (S1) step by step. For an atomic vapor, it is necessary to take into account the Doppler broadening effect. After some lengthy calculations, we finally got the fifth-order nonlinear susceptibility of the light-atom interaction displayed in Fig. S1, which has the form of

$$\chi^{(5)}(\delta_2, \delta_3) = \int_{-\infty}^{\infty} dv \frac{2N\mu_{13}\mu_{24}\mu_{23}\mu_{14}^3 f(v)}{\varepsilon_0 \hbar^5 \left\{ (\Gamma_{31} + i\Delta_{D1}) [(\Gamma_{21} + iW_{D-}\delta_2 + iW_{D+}\delta_3)(\Gamma_{41} + iW_{D-}\delta_2 + iW_{D+}\delta_3 + i\Delta_{D2}) + |\Omega_2|^2] \right.} \quad (S2)$$

$$\left. \times [(\Gamma_{11} + iW_{D+}\delta_3)(\Gamma_{41} + iW_{D+}\delta_3 + i\Delta_{D3}) + |\Omega_3|^2] \right\}$$

Here,  $f(v) = \sqrt{\frac{m_{\text{Rb}}}{2\pi k_B T}} e^{-\frac{m_{\text{Rb}} v^2}{2k_B T}}$  is the Maxwell-Boltzmann velocity distribution of the Rb atoms in thermal motion, where  $m_{\text{Rb}}$  is the mass of the Rb atom,  $k_B$  is the Boltzmann constant,  $T$  is the vapor temperature, and  $v$  is the atomic kinetic velocity;  $N$  denotes the atomic density;  $\mu_{ij}$  ( $i, j = 1, 2, 3, 4$ ) represents the electric dipole matrix element for the atomic transition  $|i\rangle \rightarrow |j\rangle$ ;  $\varepsilon_0$  stands for the vacuum permittivity;  $\Gamma_{ij}$  is the decay or decoherence rate between levels  $|i\rangle$  and  $|j\rangle$ ;  $\Delta_{D1} = \Delta_1 + v\omega_{31}/c$ ,  $\Delta_{D2} = \Delta_2 - v\omega_{42}/c$ , and  $\Delta_{D3} = \Delta_3 + v\omega_{42}/c$  with frequency detunings  $\Delta_1 = \omega_{31} - \omega_1$ ,  $\Delta_2 = \omega_{42} - \omega_2$ ,  $\Delta_3 = \omega_{42} - \omega_3$ , and  $\omega_{ij}$  being the frequency difference between  $|i\rangle$  and  $|j\rangle$ ;  $W_{D\pm} = 1 \pm v/c$  with  $c$  the speed of light in vacuum;  $\Omega_2$  and  $\Omega_3$  are the Rabi frequencies;  $\delta_2$  and  $\delta_3$  define the spectral distributions with respect to the central frequencies of the emitted  $E_{S2}$  and  $E_{S3}$  photons, respectively. Owing to the energy conservation in SSWM, the triggers of these two photons require the detection of the output  $E_{S1}$  photon at frequency  $\omega_{S1} = \omega_1 + \omega_2 + \omega_3 - \omega_{S2} - \omega_{S3}$ , which alternatively implies the spectral distributions of the entangled three-photon state to satisfy the condition of  $\delta_1 + \delta_2 + \delta_3 = 0$ . We notice that when  $T = 80^\circ\text{C}$ , the Doppler width is estimated to be about  $\Delta_D = 555$  MHz, orders of magnitude larger than the Rb natural linewidth; the atomic density is  $N = 1.2 \times 10^{11} \text{ cm}^{-3}$ ; the optical depth (OD),  $OD = N\sigma_{41}L$ , has a value of 4.6, where  $\sigma_{41} = \frac{\omega_{41}|\mu_{14}|^2}{2\varepsilon_0 \hbar c \Gamma_{41} \Delta_D} = 3\pi N \Gamma_{41} c^2 L / 2\Delta_D \omega_{41}^2$  is the on-resonance absorption cross-section of the transition  $|1\rangle \rightarrow |4\rangle$ . When  $T = 115^\circ\text{C}$ , the OD grows to the value of 45.7.

In accordance with our previous theoretical studies [1-16], the temporal correlations of the generated triphotons are expected to be governed by two folds of factors: one is the spectral profile of the fifth-order nonlinear susceptibility  $\chi^{(5)}$  given in Eq. (S2) and the other is the longitudinal phase-mismatch function (which shall be discussed subsequently). Therefore, we first look at the structure of  $\chi^{(5)}$ . Similar to our previous analysis [1-15], the resonances arising from the denominator of  $\chi^{(5)}$  in Eq. (S2) are centered around  $\delta_{1\pm} = (\Delta_{D2} \pm \Omega_{E_2})/2(1 - \frac{v}{c})$ ,  $\delta_{2\pm\pm} = (\Delta_{D3} - \Delta_{D2} \pm \Omega_{E_2} \pm \Omega_{E_3})/2(1 + \frac{v}{c})$ , and  $\delta_{3\pm} = (-\Delta_{D3} \pm \Omega_{E_3})/2(1 - \frac{v}{c})$ , where the effective

Rabi frequencies are redefined as  $\Omega_{E_2} = \sqrt{\Delta_{D2}^2 + 4|\Omega_2|^2 + 4\Gamma_{21}\Gamma_{41}}$  and  $\Omega_{E_3} =$

$\sqrt{\Delta_{D3}^2 + 4|\Omega_3|^2 + 4\Gamma_{11}\Gamma_{41}}$  with  $\Omega_2$  and  $\Omega_3$  being the original Rabi frequencies of the  $E_2$  and  $E_3$  fields, respectively. The effective linewidths of these resonances are determined by the imaginary parts of the denominator, which are found to be  $\Gamma_{\delta_2} = \frac{\Gamma_{21} + \Gamma_{41}}{2} + \frac{\Gamma_{21}\Delta_{D2}}{\Delta_{D2} + \Omega_{E2}}$  and  $\Gamma_{\delta_3} = \frac{\Gamma_{11} + \Gamma_{41}}{2} + \frac{\Gamma_{11}\Delta_{D3}}{\Delta_{D3} + \Omega_{E3}}$ . These effective linewidths naturally give rise to the temporal correlation lengths between generated triphotons. Obviously, both the resonance centers and effective linewidths are velocity-dependent and subject to the Doppler broadening effect. From the calculated  $\delta_{1\pm}$ ,  $\delta_{2\pm\pm}$  and  $\delta_{3\pm}$ , we expect that there will be in general four sets of indistinguishable SSWM processes to produce time-energy-entangled W-triphotons. As a representative example, Fig. S2 presents  $\chi^{(5)}$  under different scenarios. As one can see, after accomplishing the velocity integration, for the low OD, four distinct resonances will usually appear (see Figs. S2A and B); while for the high OD, it is possible to degenerate four resonances into two (see Fig. S2C).

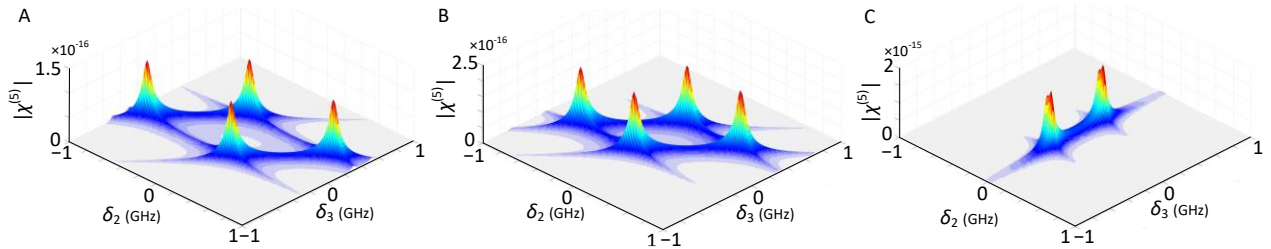


**Fig. S2 | Representative illustration of the fifth-order nonlinear susceptibility  $\chi^{(5)}$  under different parameter settings.** (A)  $\chi^{(5)}$  of Fig. 2A in the main text with the following simulation parameters:  $\Gamma_{31} = \Gamma_{41} = 2\pi \times 6$  MHz,  $\Gamma_{11} = \Gamma_{22} = 0.4 \times \Gamma_{41}$ ,  $\Gamma_{21} = 0.2 \times \Gamma_{41}$ ,  $\Delta_1 = -2$  GHz,  $\Delta_2 = -150$  MHz,  $\Delta_3 = 50$  MHz,  $OD = 4.6$ ,  $\Omega_1 = 300$  MHz,  $\Omega_2 = 870$  MHz, and  $\Omega_3 = 533$  MHz for the input laser powers  $P_1 = 4$  mW,  $P_2 = 40$  mW, and  $P_3 = 15$  mW. (B)  $\chi^{(5)}$  of Fig. 3A in the main text with the same simulation parameters as (A) except  $\Omega_2 = 533$  MHz, for the input power  $P_2 = 15$  mW. (C)  $\chi^{(5)}$  of Fig. 3D in the main text with the same simulation parameters as (B) except  $OD = 45.7$ .

### Qualitative Derivations of Linear Susceptibilities $\chi$

In addition to the resonance linewidths set by  $\chi^{(5)}$ , the triphoton temporal correlation is also dependent on the dispersion, which is determined by the linear optical response. After some calculations, the respective linear susceptibilities of the new  $E_{S1}$ ,  $E_{S2}$  and  $E_{S3}$  fields are found to be

$$\chi_{S1} \approx 0, \quad (S3)$$

$$\chi_{S2} = \int f(v) \frac{-i4N\mu_{24}^2 \left( (1 - \frac{v}{c})\delta_2 + i\Gamma_{22} \right)}{\epsilon_0 \hbar \left[ 4 \left( (1 - \frac{v}{c})\delta_2 - \Delta_{D2} + i\Gamma_{42} \right) \left( (1 - \frac{v}{c})\delta_2 + i\Gamma_{22} \right) + |\Omega_2|^2 \right]} dv, \quad (S4)$$

$$\chi_{S3} = \int f(v) \frac{-i4N\mu_{14}^2 \left( (1 + \frac{v}{c})\delta_3 + i\Gamma_{11} \right)}{\epsilon_0 \hbar \left[ 4 \left( (1 + \frac{v}{c})\delta_3 - \Delta_{D3} + i\Gamma_{41} \right) \left( (1 + \frac{v}{c})\delta_3 + i\Gamma_{11} \right) + |\Omega_3|^2 \right]} dv. \quad (S5)$$

Eq. (S3) is well justified by the weak input  $E_1$  beam and its associated large red detuning  $\Delta_1 = -2$  GHz from the transition  $|1\rangle \rightarrow |2\rangle$ . This result indicates that the group velocity of the  $E_{S1}$  photons approximately coincides with the speed of light in vacuum,  $c$ . In Fig. S3, we have provided some

numerical simulations of  $\chi_{S2}$  and  $\chi_{S3}$  to show how their profiles look like. The group velocities experienced by the  $E_{S2}$  and  $E_{S3}$  photons can be routinely obtained by

$$v_{S2} = \left( \frac{dk_{S2}}{d\omega} \right)^{-1} = \frac{c}{1 + \delta_2 \left( \frac{dn_{S2}}{d\delta_2} \right)}, \quad (\text{S6})$$

$$v_{S3} = \left( \frac{dk_{S3}}{d\omega} \right)^{-1} = \frac{c}{1 + \delta_3 \left( \frac{dn_{S3}}{d\delta_3} \right)}, \quad (\text{S7})$$

where  $n_{S2} = \sqrt{1 + \text{Re}[\chi_{S2}]}$  and  $n_{S3} = \sqrt{1 + \text{Re}[\chi_{S3}]}$  are refractive indices. The imaginary parts of  $\chi_{S2}$  and  $\chi_{S3}$  tell the linear Raman gain or absorption undergone by the  $E_{S2}$  and  $E_{S3}$  photons when they traverse the medium. With these in mind, it is not difficult to compute the longitudinal phase mismatch in the SSWM process, which is

$$\Delta k(\delta_2, \delta_3) = k_{S1} - k_{S2} + k_{S3} - k_1 + k_2 - k_3, \quad (\text{S8})$$

with  $k_j = \bar{k}_j + \frac{\omega}{v_j}$  ( $j = 1, 2, 3, S1, S2, S3$ ) and  $\bar{k}_j$  the central wavenumber.  $\Delta k$  in Eq. (S8) gives the natural spectral width for the generated triphoton state. In other words, it naturally defines the temporal coherence time by means of the light propagation effect.

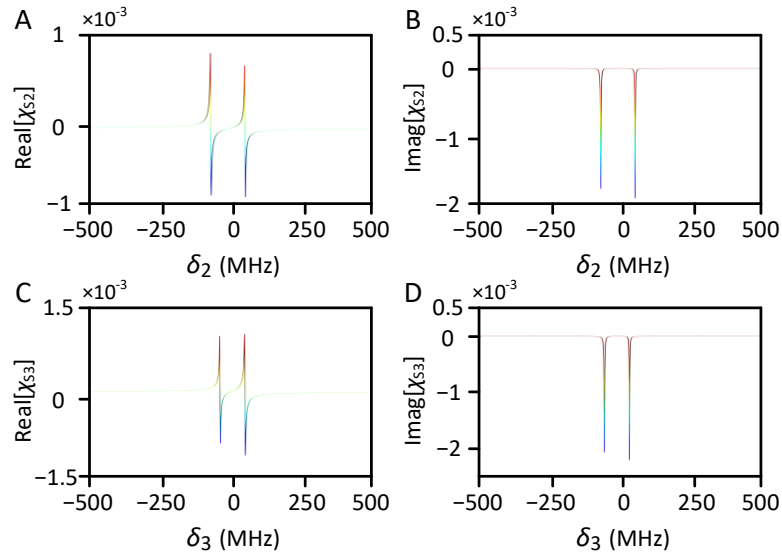


**Fig. S3 | Representative examples of linear susceptibilities  $\chi_{S2}$  and  $\chi_{S3}$ .** The involved parameters here are same as those employed in **Fig. S2B**. (**A & B**) The real and imaginary part of  $\chi_{S2}$ . (**C & D**) The real and imaging part of  $\chi_{S3}$ .

To get a sense how  $\chi_{S2}$  and  $\chi_{S3}$  behave, in Fig. S3 we use one example to qualitatively illustrate their real and imaginary parts after accomplishing the Doppler integration. As one can see,  $\chi_{S2}$  and  $\chi_{S3}$  are usually associated with two resonance structures as displayed in Figs. S3A–D. This is different from the four resonances of  $\chi^{(5)}$  in Figs. S2A and B. This difference physically stems from the adopted qualitative model to calculate linear (and nonlinear) susceptibilities. Currently,

we are working on the exact theoretical calculations of both linear and nonlinear optical responses using the accurate model developed by Wen et al, and the results will be published elsewhere.

### **Derivation of the Triphoton State $|\Psi\rangle$**

To calculate the three-photon state created from the SSWM process at the output surface of the medium, we shall work in the interaction picture and start with the effective Hamiltonian, which assumes the form of

$$H = \int_0^L dz \varepsilon_0 \chi^{(5)} E_1^{(+)} E_2^{(+)} E_3^{(+)} E_{S1}^{(-)} E_{S2}^{(-)} E_{S3}^{(-)} + H.c., \quad (S9)$$

where  $H.c.$  means the Hermitian conjugate. The electric fields of the generated  $E_{S1}$ ,  $E_{S2}$  and  $E_{S3}$  photons are described by the quantized fields,

$$E_{Sj}^{(+)} = \sum_{k_{Sj}} E_{Sj} a_j e^{i(k_{Sj}z - \omega_{Sj}t)}, \quad (S10)$$

where  $a_j$  is the annihilation operator for the mode with the wavenumber  $k_{Sj}$  and angular frequency  $\omega_{Sj}$  and  $E_{Sj} = i \sqrt{\hbar \omega_{Sj} / 2 \varepsilon_0 n_{Sj}^2 L}$ . On the other hand, we take the three input lasers  $E_1$ ,  $E_2$  and  $E_3$  to be classical plane waves,

$$E_1^{(+)} = E_1 e^{i(k_1 z - \omega_1 t)}, E_2^{(+)} = E_2 e^{i(-k_2 z - \omega_2 t)}, \text{ and } E_3^{(+)} = E_3 e^{i(k_3 z - \omega_3 t)}. \quad (S11)$$

The state vector of the triphotons can then be derived from first-order perturbation theory [1-17], which is

$$|\Psi\rangle = \frac{-i}{\hbar} \int_{-\infty}^{+\infty} dt H |0\rangle, \quad (S12)$$

with  $|0\rangle$  being the initial vacuum state. By applying Eqs. (S9)–(S12) and retaining only the terms of interest, the triphoton state (S12) formally takes the form of

$$|\Psi\rangle = \sum_{k_{S1}} \sum_{k_{S2}} \sum_{k_{S3}} F(k_{S1}, k_{S2}, k_{S3}) a_{k_{S1}}^\dagger a_{k_{S2}}^\dagger a_{k_{S3}}^\dagger |0\rangle, \quad (S13)$$

where the three-photon spectral function  $F$  is defined as

$$F(k_{S1}, k_{S2}, k_{S3}) = A \chi^{(5)} \Phi(\Delta k L) \delta(\omega_1 + \omega_2 + \omega_3 - \omega_{S1} - \omega_{S2} - \omega_{S3}), \quad (S14)$$

with  $A$  being a grouped constant. In Eq. (S14), the Dirac  $\delta$  function comes from the time integral in the steady-state approximation, and physically it assures the energy conservation in the SSWM process. From the viewpoint of atomic population, the energy conservation implies that after completing one triphoton generation, the population shall finish one cycle and return to its initial ground state  $|1\rangle$ .  $\Phi(\Delta k L)$  is termed as the longitudinal phase-mismatch function and it has the form of

$$\Phi(\Delta kL) = \frac{1-e^{-i\Delta kL}}{i\Delta kL} = \text{sinc}\left(\frac{\Delta kL}{2}\right) e^{-i\Delta kL/2}. \quad (\text{S15})$$

Due to the Doppler effect in  $\chi^{(5)}$  and  $\Delta k$ , it becomes generally difficult to have an exact analytical expression of the triphoton state (S13). Instead, hereafter we will resort to the numerical analysis on the triphoton properties.

### **Derivations of Temporal Correlation of W Triphotons**

Optical properties of the W-type triphotons can be well understood by looking at the photon statistics through the photon-counting measurement. As such, we research the triphoton temporal correlation by calculating the Glauber second-order and third-order correlation functions. This in turn suggests us to investigate the conditioned two-photon coincidence counts and the three-photon coincidence counts.

In line with the experimental setup of Fig. 1 given in the main text, the averaged triphoton coincidence counting rate reads as

$$R_3 = \lim_{T \rightarrow \infty} \frac{1}{T} \int_0^T dt_1 \int_0^T dt_2 \int_0^T dt_3 \langle \Psi | E_{S1}^{(-)}(\tau_1) E_{S2}^{(-)}(\tau_2) E_{S3}^{(-)}(\tau_3) E_{S3}^{(+)}(\tau_3) E_{S2}^{(+)}(\tau_2) E_{S1}^{(+)}(\tau_1) | \Psi \rangle, \quad (\text{S16})$$

and the two-photon coincidence counting rate is

$$R_2 = \lim_{T \rightarrow \infty} \frac{1}{T} \int_0^T dt_1 \int_0^T dt_2 \langle \Psi | E_{S2}^{(-)}(\tau_2) E_{S3}^{(-)}(\tau_3) E_{S3}^{(+)}(\tau_3) E_{S2}^{(+)}(\tau_2) | \Psi \rangle, \quad (\text{S17})$$

by assuming the  $E_{S1}$  photons to be traced away for example. In Eqs. (S16) and (S17),  $E_{Sj}^{(+)}(\tau_j)$  ( $j = 1, 2, 3$ ) is the positive frequency part of the free-space electric field evaluated at the  $j$ th detector's spatial coordinate  $r_j$  and trigger time  $t_j$  with  $\tau_j = t_j - r_j/c$ . For the sake of simplicity, we take the efficiencies of all single-photon detectors to be unity. On the other hand, the narrow bandwidths (less than GHz) of the triphotons considered here are comparable to or smaller than the spectral width of the employed single-photon detectors in our experiment. We thus can simplify Eqs. (S16) and (17) to

$$R_3 = \left| \langle 0 | E_{S3}^{(+)}(\tau_3) E_{S2}^{(+)}(\tau_2) E_{S1}^{(+)}(\tau_1) | \Psi \rangle \right|^2 = |A_3(\tau_1, \tau_2, \tau_3)|^2, \quad (\text{S18})$$

$$R_2 = \sum_{k_{S1}} \left| \langle 0 | a_{k_{S1}} E_{S3}^{(+)}(\tau_3) E_{S2}^{(+)}(\tau_2) | \Psi \rangle \right|^2 = \sum_{k_{S1}} |A_2(\tau_2, \tau_3)|^2, \quad (\text{S19})$$

where  $A_3(\tau)$  is often referred to as the three-photon amplitude or the triphoton waveform. It is worth to emphasize that  $A_2(\tau)$  is also the three-photon amplitude, despite one subsystem is not detected in the experiment. Note that both  $A_3(\tau)$  and  $A_2(\tau)$  are defined with reference to the photon detections. Plugging Eq. (S13) into Eq. (S18) yields

$$A_3(\tau_1, \tau_2, \tau_3) = A_3 \sum_{k_{S1}} \sum_{k_{S2}} \sum_{k_{S3}} e^{-i(\omega_{S1}\tau_1 + \omega_{S2}\tau_2 + \omega_{S3}\tau_3)} F(k_{S1}, k_{S2}, k_{S3}). \quad (\text{S20})$$

Again, all slowly varying terms and constants have been absorbed into  $A_3$ . Similarly, substituting Eq. (S13) into Eq. (S19) gives

$$A_2(\tau_2, \tau_3) = A_2 \sum_{k_{S2}} \sum_{k_{S3}} e^{-i(\omega_{S2}\tau_2 + \omega_{S3}\tau_3)} F(k_{S1}, k_{S2}, k_{S3}), \quad (\text{S21})$$

where all the slowly varying terms and constants have been grouped into  $A_2$ , too. Additionally, to evaluate the Dirac  $\delta$  function in  $F$  (S14), we will replace the summation over a wavenumber by an angular frequency integral as usual,

$$\sum_{k_{Sj}} \rightarrow \frac{L}{2\pi} \int d\omega_{Sj} \frac{dk_{Sj}}{d\omega_{Sj}} = \frac{L}{2\pi} \int \frac{d\omega_{Sj}}{v_{Sj}}. \quad (\text{S22})$$

With use of Eqs. (S13) and (S22), the three-photon amplitude (S20) then becomes

$$A_3(\tau_{21}, \tau_{31}) = A_3 \iint d\delta_2 d\delta_3 \chi^{(5)}(\delta_2, \delta_3) \text{sinc}\left[\frac{\Delta k(\delta_2, \delta_3)L}{2}\right] e^{-i\delta_2(\tau_{21} + L/2v_{S2})} e^{-i\delta_3(\tau_{31} + L/2v_{S3})}. \quad (\text{S23})$$

The three-photon coincidence counting rate (S18) is simply module squared of  $A_3(\tau_{21}, \tau_{31})$ , i.e.,

$$R_3 = |A_3(\tau_{21}, \tau_{31})|^2.$$

From Eq. (S23), it is not difficult to see that the three-photon amplitude  $A_3(\tau_{21}, \tau_{31})$  is the convolution of the fifth-order nonlinear susceptibility  $\chi^{(5)}(\delta_2, \delta_3)$  and the longitudinal phase-mismatch function  $\Phi(\Delta kL)$ . Physically, this implies that the triphoton temporal coherence is jointly determined by these two factors. As a consequence, two distinct regions can be expected to appear in three-photon temporal correlation measurements, the so-called damped Rabi oscillation regime dominated by  $\chi^{(5)}$  and the group-delay regime dominated by  $\Phi(\Delta kL)$ . We have examined these regions in the experiment and presented some recorded data in Figs. 2–4 in the main text as well as Figs. S11 and S12 below. As a qualitative comparison, in Fig. S4 we have provided their corresponding theoretical simulations. It is easy to see that both Figs. S4A and B exhibit the three-photon coincidence counts in the damped Rabi oscillation regime, while Fig. S3C displays the case in the group-delay region, which qualitatively explain the experimental observations of Figs. 2A, 3A and 3D in the main text.

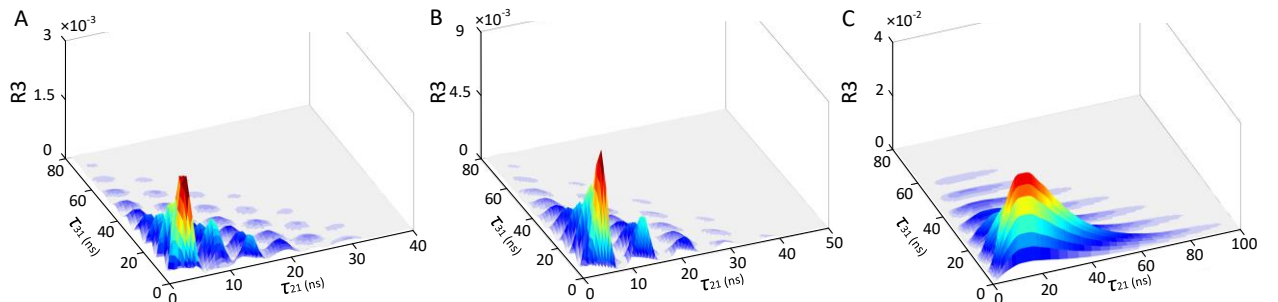


**Fig. S4 | Theoretical simulations of triphoton coincidence counting rates  $R_3$ .** (A)  $R_3$  corresponding to **Fig. 2A** in the main text with the same parameters used in **Fig. S2A**. (B)  $R_3$  corresponding to **Fig. 3A** in the main text with the same parameters used in **Fig. S2B**. (C)  $R_3$  corresponding to **Fig. 3D** in the main text with the same parameters used in **Fig. S2C**.

In the similar way, we can show that the conditioned two~photon coincidence counting rate can be evaluated by

$$R_2(\tau_{23}) = R_2 \int d\delta_3 \left| \int d\delta_2 \chi^{(5)}(\delta_2, \delta_3) \text{sinc} \left[ \frac{\Delta k(\delta_2, \delta_3)L}{2} \right] e^{-i\delta_2(\tau_{23} + L/2v_{S2})} \right|^2, \quad (\text{S24})$$

where  $\tau_{23} = \tau_2 - \tau_3$  and  $R_2$  is a grouped constant. As one can see from Eq. (S24),  $R_2(\tau_{23})$  is a function of  $\tau_{23}$ , implying the existence of a partial entanglement between the remaining  $E_{S2}$  and  $E_{S3}$  photons after tracing the  $E_{S1}$  photon away. This is clearly a signature of the property of the tripartite W class. In Eq. (S24), the second integral inside the module squared is a convolution between  $\chi^{(5)}$  and  $\Phi(\Delta kL)$ . Similarly, the functional profile of  $R_2(\tau_{23})$  is in general determined by both factors. However, if either of them plays the dominant role,  $R_2(\tau_{23})$  will showcase two distinctive scenarios, the damped Rabi oscillation regime and the group-delay regime. Other arrangements on conditional two~photon coincidence counts can be calculated by following the same reasoning. Here, we will not repeat those calculations and leave them as an exercise to the reader. In Figs. 2C and D and Figs. 3B, C, E and F in the main text, we have reported examples of such measured conditional two~photon coincidence counts. As a comparison, Fig. S5 accordingly presents their respective theoretical simulations. As one can see, our theory qualitatively agrees with the experiment.

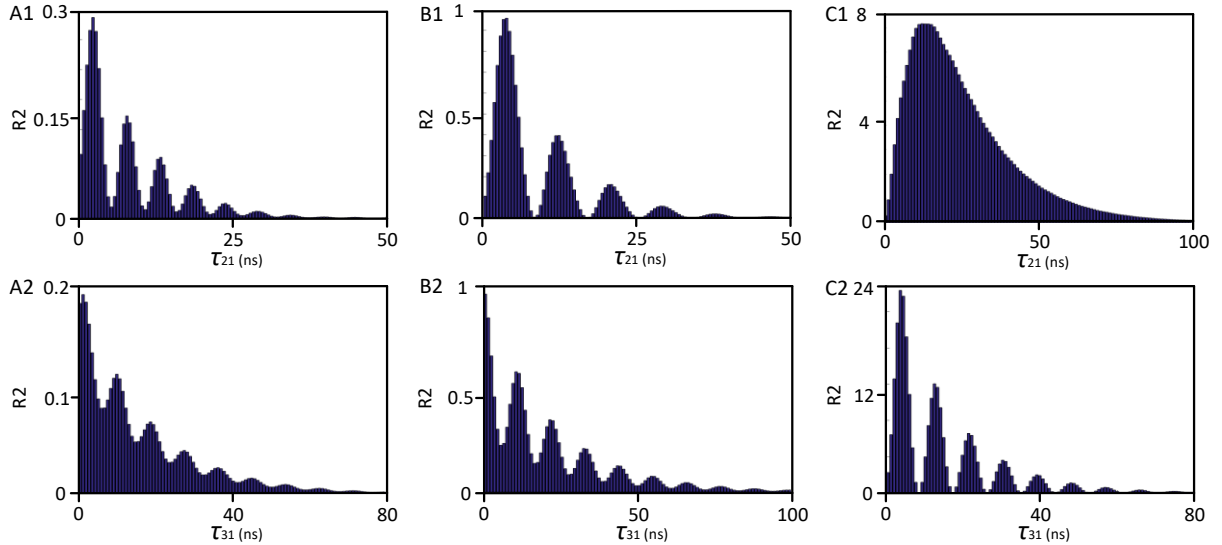


**Figure S5 | Theoretical simulations of conditional two~photon coincidence counting rates  $R_2$  for Fig. S4.** (A1)  $R_2$  by tracing the  $E_{S3}$ -photons away in **Fig. S4A**. (A2)  $R_2$  by tracing the  $E_{S2}$ -photons away in **Fig. S4A**. (B1)  $R_2$  by tracing the  $E_{S3}$ -photons away in **Fig. S4B**. (B2)  $R_2$  by tracing the  $E_{S2}$ -photons away in **Fig. S4B**. (C1)  $R_2$  by tracing the  $E_{S3}$ -photons away in **Fig. S4C**. (C2)  $R_2$  by tracing the  $E_{S2}$ -photons away in **Fig. S4C**.

## **Triphoton W State Entangled in Other Degrees of Freedom**

Although the focus of the current work is on time-energy-entangled W triphotons, in fact, they can be also entangled in other degrees of freedom including space-momentum, polarization, and orbital angular momentum. Thanks to the SSWM process vastly enhanced by atomic coherence, it allows one to explore various three-photon entanglement based on different degrees of freedom, which becomes uneasy or even impossible to achieve with previously proposed schemes or methods. Moreover, our system is capable of forming triphoton hyperentangled states by entangling more than one degree of freedom of light, which will become technically challenging for any previously reported multiphoton generation platform. The system layouts and theoretical calculations on these triphoton entangled states are out of the scope of the present work and will be discussed elsewhere. Of importance, triphotons entangled in different degrees of freedom promise distinctive quantum technological applications. For instance, the W-type triphotons with spatial correlations [19-21] can be used to achieve quantum imaging and remote sensing with sub-Rayleigh superresolution that cannot be mimicked and even accessed by biphotons or classical light, thereby making the whole phenomena indisputably quantum.

## **II. Further Information on Experimental Measurements and Data Processing**

In what follows, we would like to provide further details on the experimental measurements and data processing. We will also report more recorded experimental data on triphoton coincidences to demonstrate that, indeed, the proposed SSWM in coherent atomic ensembles is an efficient process to yield high-quality and reliable genuine triphotons. Of importance, these data plus those in the main text give a good account of the versatility of the source, which may enable new technological developments unreachable to the current photon resources.

### **Possible Biphoton Processes**

As mentioned in the Methods, one major accidental coincidence noise in three-photon correlation measurement comes from the simultaneous presence of two pairs of biphotons, from different spontaneous four-wave mixing (SFWM) processes, onto the single-photon detectors. Fortunately, these SFWMs are accompanied by different phase matching conditions, deviating from the one for the SSWM process. Moreover, the biphotons originating from these SFWMs have different central frequencies from those of the desired triphotons. As such, by carefully manipulating the phase matching conditions and employing narrowband filters, one can effectively remove these biphoton false trigger events from the genuine triphoton coincidence counts. To have an intuitive picture of these biphoton generations, in Fig. S6 we have schematically illustrated all possible SFWM processes. According to the level structure, we have identified seven such SFWM processes and depicted them in Figs. S6B–H. The biphotons produced from these SFWMs are the main source of accidental coincidences to the real measurements. In Methods, we have already elaborated on their possible combinations for potential error-triggering events.



Although entangled quadraphotons might be generated from a higher-order nonlinear wave mixing process, their emission possibility will be sufficiently low and won't become one major noise source to the triphoton detection. As such, we won't discuss them here further.

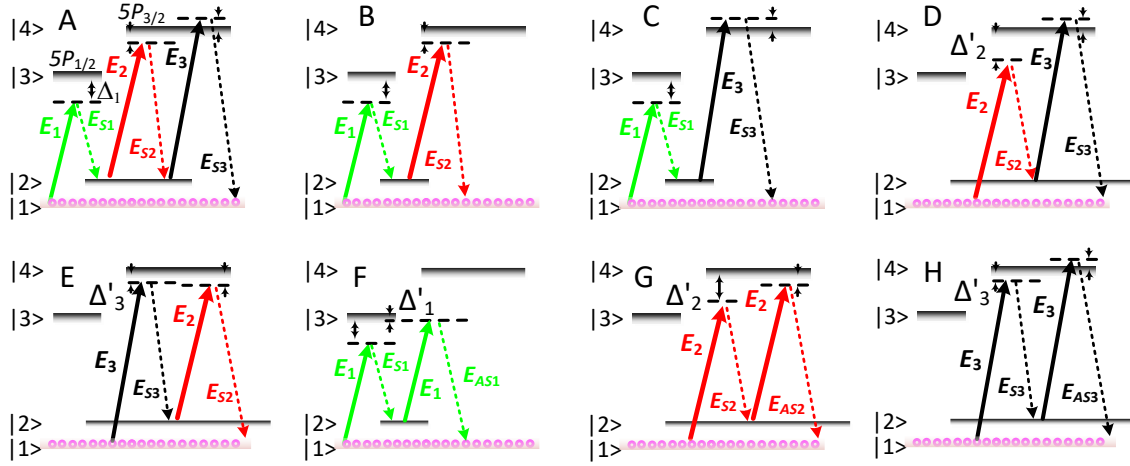


**Figure S6 | Seven possible SFWM processes which may result in accidental coincidences onto three-photon coincidence counting measurement.** (A) Atomic energy-level structure for triphoton generation. (B-H) Seven possible SFWM processes where the emitted biphotons may become accidental coincidences in the measured three-photon coincidence counts.

### Measured Coincidence Counts by Subtracting Background Accidentals

In Figs. 2 and 3 in the main text, we have presented the recorded data with background accidental counts. Here, in Fig. S7 and S8, we have processed these measured data by subtracting these background accidental counts. By comparing Figs. 2 and 3 with Fig. S7 and S8, one can see that the essential features have been well retained for both cases. In Figs. S7C, S7D, S8B, S8C and S8F, we have illustrated the oscillation periods mentioned in the main text with green and red dashed lines based on the measured data. By comparing Figs. S7C, S7D, S8B, S8C, S8E and S8F with Figs. S4A1–C2, we are aware that our qualitative mode on optical response can only provide a qualitative interpretation to the experimental results. But nevertheless, it does reveal certain key features of the measurements.

To gain a better understanding of the conditional two~photon coincidences and conditional three-photon coincidences, we have further processed the experimental data in Figs. 2A, 3A and 3D by looking at other different scenarios after removing the corresponding background accidental counts. As some typical examples, Fig. S9 reports a portion of such processed experimental data in a way by complying with specific conditions. From these figures, it is not difficult to find that the coherence length of the two~photon residual temporal correlation is not fixed and depends on the conditions of the performed measurement. This is also applicable to the coherence length of the conditional three-photon temporal correlation. All in all, these features are not available from the previous demonstrations. From another point of view, this also proves that the generated three-photon state has flexible and tunable characteristics, which are essential for its various applications.

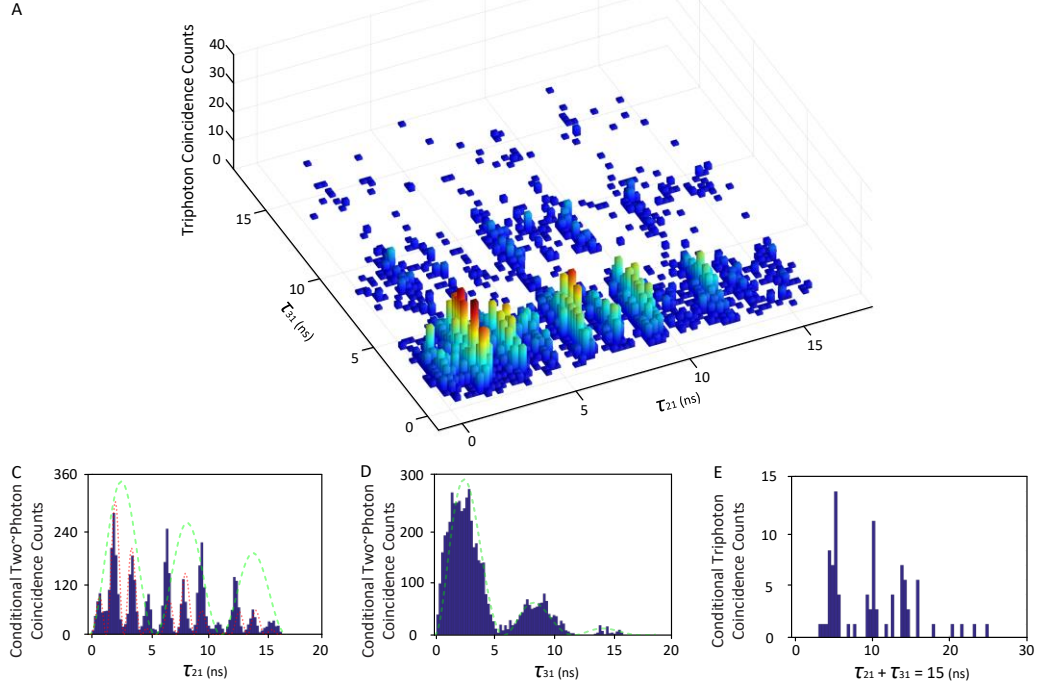


**Fig. S7 | Triphoton coincidence counts, conditioned two-photon coincidence counts, and conditional three-photon coincidence counts presented in Fig. 2 in the main text by removing background accidentals. In (C & D), the green and red dashed lines are used to illustrate periodic oscillations mentioned in the main text.**

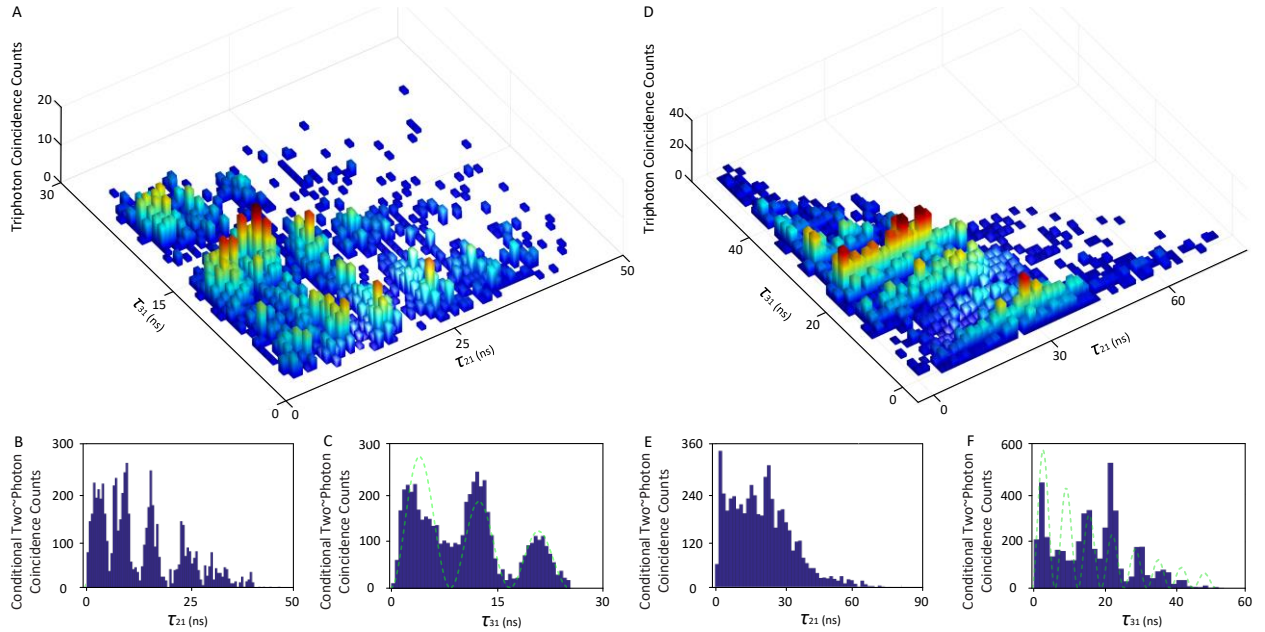


**Fig. S8 | Triphoton coincidence counts, conditioned two-photon coincidence counts, and conditional three-photon coincidence counts displayed in Fig. 3 in the main text by subtracting background accidentals. In (B, C & F), the green dashed lines are used to illustrate periodic oscillations mentioned in the main text.**

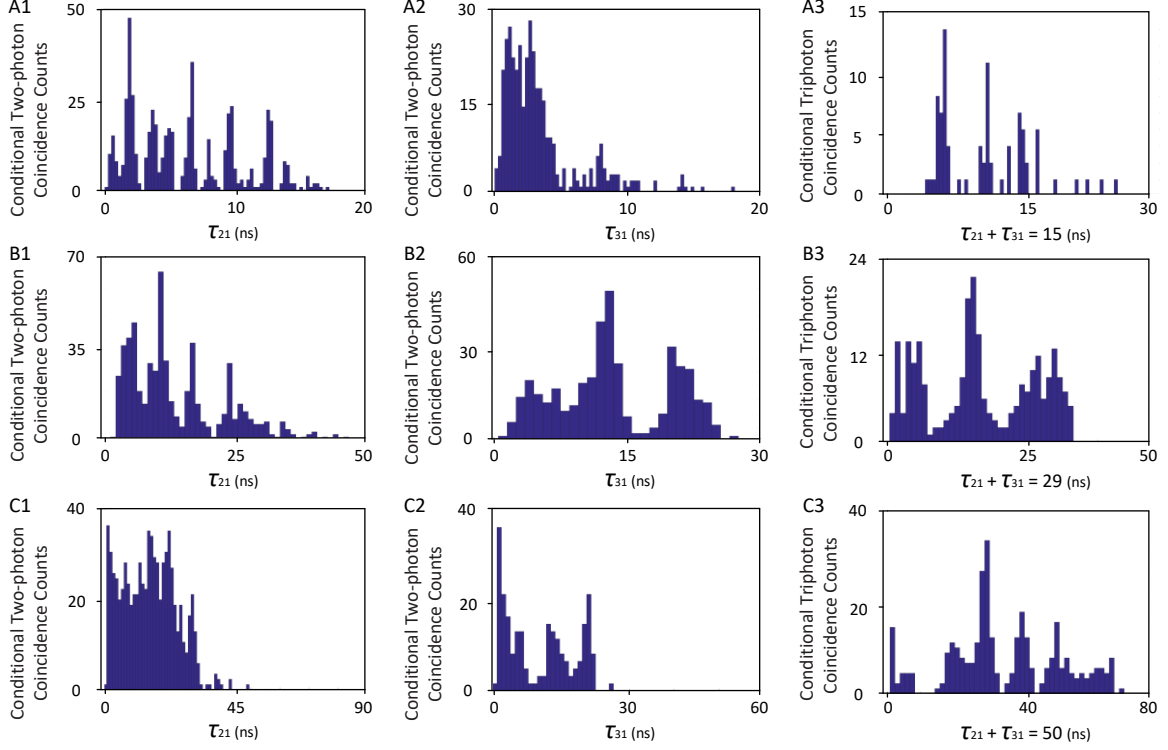


**Fig. S9 | Conditional two~photon coincidence counts  $R_2$  and conditional triphoton coincidence counts  $R_3$  by subtracting their respective background accidentals for the scenarios of Figs. 2A, 3A and 3D shown in the main text.** Specifically, (A1)  $R_2(\tau_{21})$  by fixing  $\tau_{31} = 2.6$  ns for  $R_3$  in Fig. 2A in the main text; (A2)  $R_2(\tau_{31})$  by fixing  $\tau_{21} = 2.0$  ns for  $R_3$  in Fig. 2A; (A3)  $R_3(\tau_{21} + \tau_{31} = 15.0$  ns) for  $R_3$  in Fig. 2A; (B1)  $R_2(\tau_{21})$  by fixing  $\tau_{31} = 13.0$  ns for  $R_3$  in Fig. 3A in the main text; (B2)  $R_2(\tau_{31})$  by fixing  $\tau_{21} = 4.0$  ns for  $R_3$  in Fig. 3A; (B3)  $R_3(\tau_{21} + \tau_{31} = 29.0$  ns) for  $R_3$  in Fig. 3A; (C1)  $R_2(\tau_{21})$  by fixing  $\tau_{31} = 21.0$  ns for  $R_3$  in Fig. 3D in the main text; (C2)  $R_2(\tau_{31})$  by fixing  $\tau_{21} = 31.0$  ns for  $R_3$  in Fig. 3D; (C3)  $R_3(\tau_{21} + \tau_{31} = 50.0$  ns) for  $R_3$  in Fig. 3D.

### **Reconstruction Procedure for Triphoton Coincidence Counts**

Unlike the standard two-photon correlation measurement, in practice, no generic three-photon coincidence circuit is commercially available in the market. As a result, each group has to build up its own three-photon coincidence circuit. As laid out in Fig. S10, we construct such a detection system based on two-photon coincidence circuits. Specifically, in a preset three-photon correlation time window, we reconstruct three collected single-photon trigger events from SPCM<sub>1</sub>, SPCM<sub>2</sub> and SPCM<sub>3</sub> through the simultaneous detection of two pairs of two-photon coincidence counts,  $\{E_{S1}, E_{S2}\}$  and  $\{E_{S1}, E_{S3}\}$ , with the help of an additional diagnose SPCM<sub>D</sub>. In the experiment, for every recorded three-photon coincidence count, we use the  $E_{S1}$ -photon click as a shared start trigger to initiate two electronic pulses  $I_1$  from SPCM<sub>1</sub>, one of which undergoes a 150-ns delay, as shown in Fig. S10A. Meantime, the detections of the  $E_{S2}$ - and  $E_{S3}$ -photon will jointly serve as the stop trigger, where the electronic pulse  $I_3$  from SPCM<sub>3</sub> will be delayed by 150 ns with respect to the electronic pulse  $I_2$  from SPCM<sub>2</sub>. With these arrangements, the  $E_{S1}$  and  $E_{S2}$  photons will be measured first as a function of  $\tau_{21}$ , and then the  $E_{S1}$  and  $E_{S3}$  photons will be recorded after 150 ns

as a function of  $\tau_{31}$ . In this way, the three-photon temporal correlations can be captured in the coincidence counting measurement. To see how each two-photon coincidence counting component works, in Fig. S10B–D we have presented one set of such experimental data collected over 5 minutes by setting the time bin width of each SPCM to be 0.25 ns. As one can see, the joint detection of the  $E_{S1}$  and  $E_{S2}$  photons gives rise to two-photon temporal correlation as a function of the relative time difference  $\tau_{21}$  between the clicks of the two involved single-photon detectors, SPCM<sub>1</sub> and SPCM<sub>2</sub> (see Fig. S10B). Similarly, the joint detection of the  $E_{S1}$  and  $E_{S3}$  photons reveals their residual temporal correlation as a function of the relative triggering time difference  $\tau_{31}$  between the clicks of the two involved single-photon detectors SPCM<sub>1</sub> and SPCM<sub>3</sub> (see Fig. S10C). Since the diagnose single-photon detector SPCM<sub>D</sub> is triggered by artificial electronic signals, the coincidence counting detection between the  $E_{S3}$  photons and artificial diagnose signals will result in no exact temporal correlation as reflected in Fig. S10D.

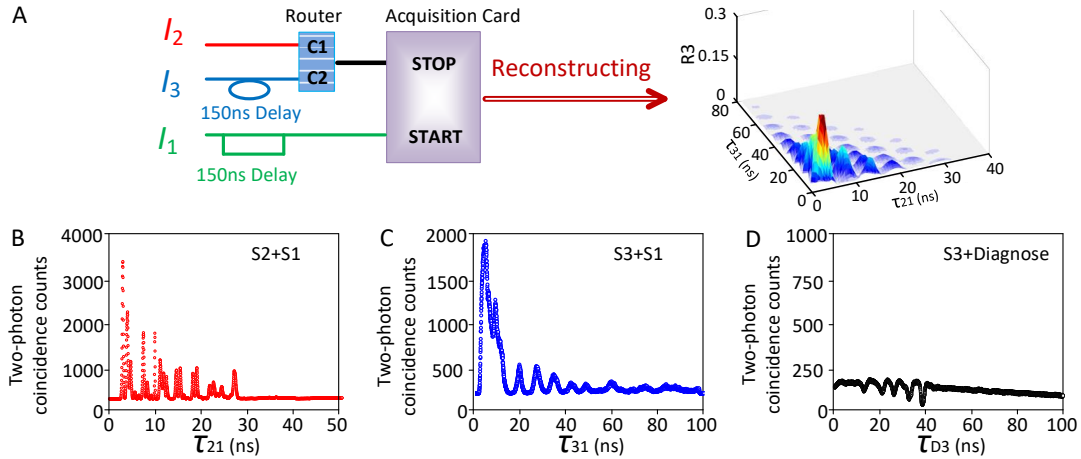


**Fig. S10 | Three-photon detection system and coincidence counting reconstruction.** (A) Schematic of our home-made detection system enabling three-photon coincidence counting reconstruction. As an example, (B–D) exhibit the recorded two-photon coincidence counts in one experiment, respectively, by SPCM<sub>1</sub> and SPCM<sub>2</sub>, SPCM<sub>1</sub> and SPCM<sub>3</sub>, and SPCM<sub>3</sub> and SPCM<sub>D</sub> as functions of the relative time differences  $\tau_2$ ,  $\tau_3$  and  $\tau_d$  between the clicks of the two involved single-photon detectors. The experimental data was collected over 5 minutes by setting the bin width of each SPCM to be 0.25 ns. Other parameters are  $P_1 = 4$  mW,  $P_2 = 40$  mW,  $P_3 = 15$  mW,  $\Delta_1 = -2$  GHz,  $\Delta_2 = -150$  MHz,  $\Delta_3 = 50$  MHz,  $\Omega_1 = 300$  MHz,  $\Omega_2 = 870$  MHz,  $\Omega_3 = 533$  MHz.

Experimentally, to catch genuine triphotons in detection, it is very important to optimize the phase-matching conditions of the SSWM process by controlling the wavelengths and injection angles of three input optical driving beams as well as the triphoton collection directions. Other than these arrangements, to ensure that the detected triphotons indeed come from the desired SSWM process, we have further implemented an additional coincidence counting detection by jointly measuring the  $E_{S3}$  photons with the artificially introduced diagnose signals from SPCM<sub>D</sub> in simultaneous conjunction with the joint detection of the  $E_{S1}$  and  $E_{S2}$  photons. By applying the same reconstruction method described above, we have obtained only a few accidental coincidences per

minute when using the two-photon coincidences  $\{E_{S1}, E_{S2}\}$  and  $\{E_{S3}, E_D\}$  to construct the three-photon histogram, indicating that, indeed, no true quantum correlation shall exist in any two pairs of uncorrelated two-photon coincidences.

### **Additional Experimental Data**

In the experiment, we have carried out a series of three-photon coincidence counting measurements by changing the system parameters. In addition to the data illustrated in Figs. 2 and 3 in the main text, here we would like to show another group of measured data. As plotted in Fig. S11, we collected the three-photon coincidence trigger events over 1 h with the time bin width of each SPCM to be set at 2.0 ns. Most of the experimental parameters are same as those of Fig. 2A in the main text except  $P_2 = 7$  mW,  $P_3 = 7$  mW, and  $OD = 45.7$ . According to the recorded data, we found that the triphoton production rate is  $100 \pm 11$  per minute but with the background accidentals of  $8 \pm 3.1$  per minutes. Also in such a case, the triphoton temporal correlation falls into the group-delay regime. This can be well verified by examining the conditional two~photon correlations by tracing either one photon away from every triphoton. In Fig. S11B and C, we have presented such conditional two~photon coincidence counts. As one can see, the Rabi oscillations almost disappear in these two figures.

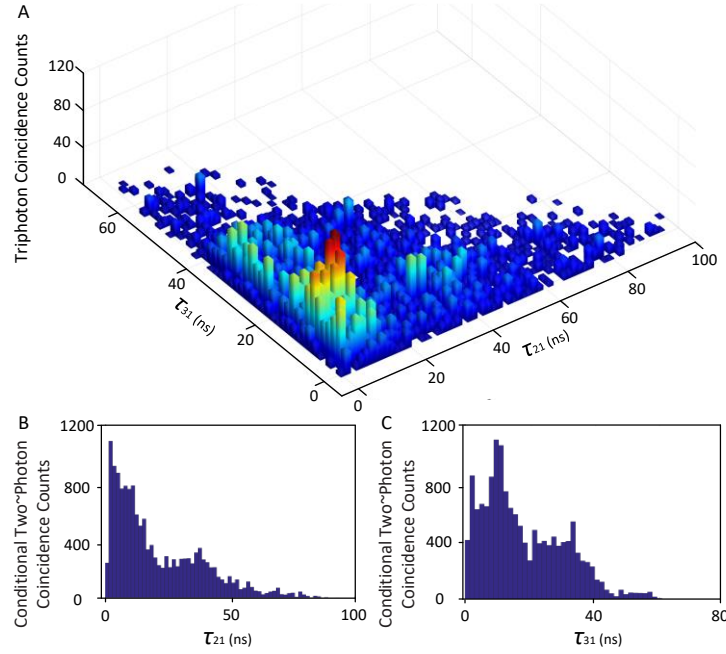


**Fig. S11 | Triphoton temporal correlation in the group-delayed region.** (A) The histogram of three-photon coincidence counts over 1 hour with 2.0-ns time-bin width for each single-photon detector. The triphoton overall generation rate reads as  $100 \pm 11$  per minute with the measured background accidental coincidences to be  $8 \pm 3.1$  per minute. (B & C) Conditional two~photon coincidence counts by tracing the  $E_{S3}$  or  $E_{S2}$  photons away from each three-photon joint trigger event in (A). The experimental parameters are same as those of Fig. 2A in the main text except for  $P_2 = 7$  mW,  $P_3 = 7$  mW,  $\Omega_2 = 364$  MHz,  $\Omega_3 = 364$  MHz, and  $OD = 45.7$ .

In Fig. S12, we have reported another set of measurements in the group-delay region. In comparison to Fig. S11, one can see that the small oscillations in the previous figures are largely suppressed.

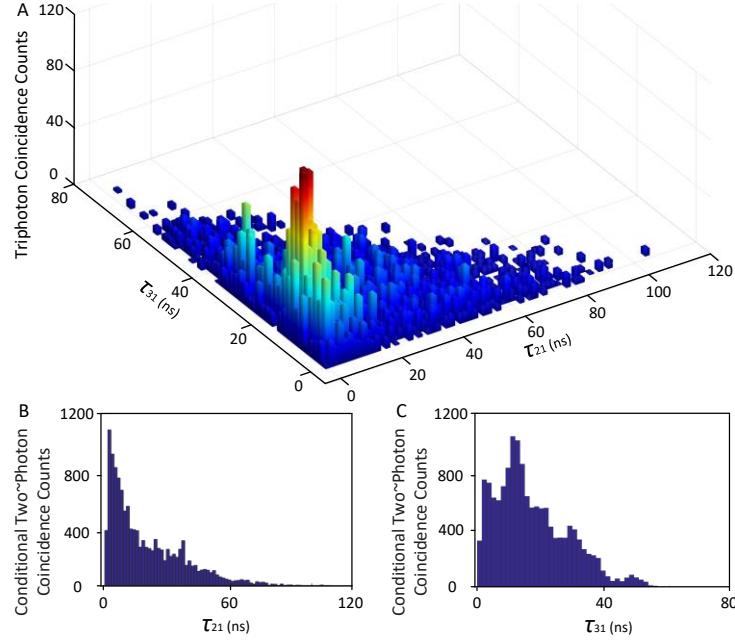


**Fig. S12 | Triphoton temporal correlation in the group-delayed region.** (A) The histogram of three-photon coincidence counts over 1.5 hours with 1.5-ns time bin width for each single-photon detector. The triphoton overall generation rate reads as  $140 \pm 15$  per minute with the measured background accidental coincidences to be  $13 \pm 3.4$  per minute. (B & C) Conditional two~photon coincidence counts by tracing the  $E_{S3}$  or  $E_{S2}$  photons away from each three-photon joint trigger event in (A). The experimental parameters are same as those of **Fig. 2A** in the main text except for  $P_2 = 6$  mW,  $P_3 = 6$  mW,  $\Omega_2 = 351$  MHz,  $\Omega_3 = 351$  MHz, and  $OD = 45.7$ .

### III. Comparison of Various Mechanisms on Multiphoton Generation

In this session, we have summarized most of the major experimental demonstrations on entangled three-photon and multi-photon generation reported so far, and have tabulated their critical parameters and achieved optical properties in TABLE I for comparison.

Degree of freedom	Counts per hour	Class	Year (reference)
Path	24	3-photon GHZ	<i>Phys. Rev. Lett.</i> <b>82</b> , 1345-1349 (1999)
Path	69	4-photon GHZ	<i>Phys. Rev. Lett.</i> <b>86</b> , 4435-4439 (2001)
Path	3600	4-photon Dicke	<i>Phys. Rev. Lett.</i> <b>98</b> , 063604 (2007)
Energy-time	$6.2 \pm 0.55$	3-photon	<i>Nature</i> <b>466</b> , 601-603 (2010)



Energy-time	7	3-photon	<i>Nat. Phys.</i> <b>9</b> , 19-22 (2013)
Polarization	744±150	3-photon	<i>Nat. Photon.</i> <b>8</b> , 801-807 (2014)
Path	10	5-photon	<i>Nature</i> <b>430</b> , 54-58 (2004)
Polarization	5220	3-photon W	<i>Phys. Rev. Lett.</i> <b>95</b> , 150404 (2005)
Polarization	300	4-Photon	<i>Phys. Rev. Lett.</i> <b>90</b> , 200403 (2003)
Polarization	175	4-Photon	<i>Phys. Rev. Lett.</i> <b>92</b> , 107901 (2004)

#### IV. Further Discussion on the Reported Triphoton Source

It is instructive to look at whether the reported triphoton source would be able to produce the GHZ-type triphotons entangled in time-energy (and other degrees of freedom) [22,23]. To the best of our knowledge, so far there is no single proposal on direct generation of continuous-mode time-energy-entangled GHZ triphotons in the literature. This is due to the fact that, in order to create such a three-photon GHZ state, two of them must be degenerate in every degree of freedom [22]. For our triphoton source, you might be wondering what if two of them are arranged into a degenerate state, would we form a GHZ state? In theory, this is viable. But technically, an experiment of such will be highly challenging.

#### References

- [1] Wen, J., Du, S. & Rubin, M. H. Biphoton generation in a two-level atomic ensemble. *Phys. Rev. A* **75**, 033809 (2007).
- [2] Wen, J., Du, S. & Rubin, M. H. Spontaneous parametric down-conversion in a three-level system. *Phys. Rev. A* **76**, 013825 (2007).
- [3] Wen, J., Du, S., Zhang, Y., Xiao, M. & Rubin, M. H. Nonclassical light generation via a four-level inverted-Y system. *Phys. Rev. A* **77**, 033816 (2008).
- [4] Zhang, D., Cai, Y., Zheng, Z., Barral, D., Zhang, Y., Xiao, M. & Bencheikh, K. Non-Gaussian nature and entanglement of spontaneous parametric nondegenerate triple-photon generation. *Phys. Rev. A* **103**, 013704 (2021).
- [5] Li, K., Cai, Y., Wu, J., Liu, Y., Xiong, S., Li, Y. & Zhang, Y. Three-body topology entanglement generation via a six-wave mixing: Competing and coexisting of linear and nonlinear optical responses in triphoton temporal correlation. *Adv. Quantum Technol.* **3**, 1900119 (2020).
- [6] Nie, Z., Zheng, H., Li, P., Yang, Y., Zhang, Y. & Xiao, M. Interacting multiwave mixing in a five-level atomic system. *Phys. Rev. A* **77**, 063829 (2008).
- [7] Chen, H. X., Qin, M. Z., Zhang, Y. Q., Zhang, X., Wen, F., Wen, J. & Zhang, Y. Parametric amplification of dressed multi-wave mixing in an atomic ensemble. *Laser. Phys. Lett.* **11**, 045201 (2014).

- [8] Li, K., Zhang, D., Raza, F., Zhang, Z., Puttapirat, P., Liu, Y. & Zhang, Y. Multi-contact switch using double-dressing regularity of probe, fluorescence, and six-wave mixing in a Rydberg atom. *J. Chem. Phys.* **149**, 074310 (2018).
- [9] Wen, J., Oh, E. & Du, S. Tripartite entanglement generation via four-wave mixings: narrowband triphoton W state. *J. Opt. Soc. Am. B* **27**, A11-A20 (2010).
- [10] Yun, S., Wen, J., Xu, P., Xiao, M. & Zhu, S. N. Generation of frequency-correlated narrowband biphotons from four-wave mixing in cold atoms. *Phys. Rev. A* **82**, 063830 (2010).
- [11] Wen, J., Zhai, Y. H., Du, S. & Xiao, M. Engineering biphoton wave packets with an electromagnetically induced grating. *Phys. Rev. A* **82**, 043814 (2010).
- [12] Du, S., Wen, J. & Rubin, M. H. Narrowband biphoton generation near atomic resonance. *J. Opt. Soc. Am. B* **25**, C98-C108 (2008).
- [13] Du, S., Oh, E., Wen, J. & Rubin, M. H. Four-wave mixing in three-level systems: Interference and entanglement. *Phys. Rev. A* **76**, 013803 (2007).
- [14] Du, S., Wen, J., Rubin, M. H. & Yin, G. Y. Four-wave mixing and biphoton generation in a two-level system. *Phys. Rev. Lett.* **98**, 53601 (2007).
- [15] Wen, J. & Rubin, M. H. Transverse effects in paired-photon generation via an electromagnetically induced transparency medium. I. Perturbation theory. *Phys. Rev. A* **74**, 023808 (2006).
- [16] Keller, T. E., Rubin, M. H., Shih, Y. & Wu, L.-A. Theory of the three-photon entangled state. *Phys. Rev. A* **57**, 2076-2079 (1998).
- [17] Rubin, M. H., Klyshko, D. N., Shih, Y.-H. & Sergienko, A. V. Theory of two-photon entanglement in type-II optical parametric down-conversion. *Phys. Rev. A* **50**, 5122-5133 (1994).
- [18] Klyshko, D. N. *Photons and Nonlinear Optics* (Gordon and Breach, 1988).
- [19] Wen, J., Xu, P., Rubin, M. H. & Shih, Y. Transverse correlation in triphoton entanglement: Geometrical and physical optics. *Phys. Rev. A* **76**, 023828 (2007).
- [20] Wen, J., Rubin, M. H. & Shih, Y. Transverse correlation in multiphoton entanglement. *Phys. Rev. A* **76**, 45802 (2007).
- [21] Wen, J., Du, S. & Xiao, M. Improving spatial resolution in quantum imaging beyond the Rayleigh diffraction limit using multiphoton W entangled states. *Phys. Lett. A* **374**, 3908-3911 (2010).
- [22] Wen, J. & Rubin, M. H. Distinction of tripartite Greenberger-Horne-Zeilinger and W states entangled in time (or energy) and space. *Phys. Rev. A* **79**, 025802 (2009).
- [23] Wen, J., Rubin, M. H. & Shih, Y. H. Spatial resolution enhancement in quantum imaging beyond the diffraction limit using entangled photon-number state. arXiv:0812.2032 (2008).